Turun yliopisto
University of Turku

NEW BIOMARKERS IN GLIOMA

PET/CT imaging and the prognostic value of somatostatin receptor subtype 2

Aida Kiviniemi

TURUN YLIOPISTON JULKAISUJA – ANNALES UNIVERSITATIS TURKUENSIS
Sarja - ser. D osa - tom. 1284 | Medica - Odontologica | Turku 2017

Turun yliopisto
University of Turku

NEW BIOMARKERS IN GLIOMA

PET/CT imaging and the prognostic value of somatostatin receptor subtype 2

Aida Kiviniemi

TURUN YLIOPISTON JULKAISUJA – ANNALES UNIVERSITATIS TURKUENSIS
Sarja - ser. D osa - tom. 1284 | Medica - Odontologica | Turku 2017

University of Turku

Faculty of Medicine
Department of Clinical Physiology
and Nuclear Medicine
University of Turku Doctoral
Programme of Clinical Investigation
Turku PET Centre
Turku University Hospital

Supervised by

Professor Heikki Minn, MD, PhD
Department of Oncology
and Radiotherapy,
Turku University Hospital
University of Turku
Turku, Finland

Professor Anne Roivainen, PhD
Turku PET Centre
Turku Center for Disease Modelling
University of Turku
Turku, Finland

Reviewed by

Professor Ritva Vanninen, MD, PhD
Department of Clinical Radiology,
Kuopio University Hospital
University of Eastern Finland
Kuopio, Finland

Docent Hannu Haapasalo, MD, PhD
Department of Pathology
University of Tampere
Tampere, Finland

Opponent

Docent Hanna Mäenpää, MD, PhD
Comprehensive Cancer Center,
Helsinki University Hospital
Helsinki, Finland

The originality of this thesis has been checked in accordance with the University of Turku quality assurance system using the Turnitin OriginalityCheck service.

Layout: Pia Sonck-Koota (www.sonck-koota.fi)

ISBN 978-951-29-6814-5 (PRINT)
ISBN 978-951-29-6815-2 (PDF)
ISSN 0355-9483 (Print)
ISSN 2343-3213 (Online)
Painosalama Oy - Turku, Finland 2017

To Tuomas, Kauri,
Vellamo, and Ellinoora

ABSTRACT

Aida Kiviniemi

NEW BIOMARKERS IN GLIOMA – PET/CT IMAGING AND THE PROGNOSTIC VALUE OF SOMATOSTATIN RECEPTOR SUBTYPE 2

University of Turku, Faculty of Medicine, Department of Clinical Physiology and Nuclear Medicine, Doctoral Programme of Clinical Investigation, Turku PET Centre, Turku University Hospital, Turku, Finland

Gliomas are brain tumors with dismal prognoses. They are classified based on histology and molecular biomarkers that guide therapeutic decision-making. Somatostatin receptor subtype 2- (SSTR2) targeted radionuclide therapy has been suggested as a novel treatment approach for gliomas. However, SSTR2 expression in different glioma entities is still controversial. Therefore, a method is needed for *in vivo* detection of SSTR2 in gliomas, which would help in the selection of patients for radionuclide therapy.

Aims of this doctoral thesis were 1) to study the potential of positron emission tomography/computed tomography (PET/CT) to detect SSTR2 in gliomas *in vivo*, which would benefit the planning and follow-up of SSTR2-targeted radionuclide therapy, 2) to characterize SSTR2 expression in gliomas and explore its impact on survival, and 3) to evaluate serum glial fibrillary acidic protein (GFAP) and epidermal growth factor receptor (EGFR) as circulating biomarkers.

First, animal glioma models were studied for SSTR2 expression with PET/CT, autoradiography, and immunohistochemistry. Secondly, a prospective clinical study was conducted to examine the value of SSTR2 PET/CT and serum GFAP and EGFR in 27 patients with malignant glioma. Thirdly, SSTR2 expression and its impact on survival was retrospectively evaluated in 184 patients with glioma.

SSTR2 expression was detected in experimental gliomas, but the value of SSTR2-targeted PET/CT was limited. Also, in patients with malignant glioma, PET/CT could not predict SSTR2 expression in tumor tissue. In contrast, SSTR2 expression associated with oligodendrogliomas and improved prognoses, which was confirmed in the retrospective setup. Serum GFAP correlated with glioblastomas and tumor burden, whereas circulating EGFR was not related to tumor EGFR expression.

In conclusion, SSTR2 and serum GFAP are potential new biomarkers with diagnostic, prognostic, and/or therapeutic value. SSTR2 PET/CT has limited value in selecting glioma patients for radionuclide therapy.

Keywords: Glioma, Somatostatin receptor, PET, serum GFAP, oligodendroglioma

TIIVISTELMÄ

Aida Kiviniemi

GLIOOMAN UUDET BIOMARKKERIT – SOMATOSTATIINIRESEPTORIEN PET/TT -KUVANTAMINEN JA VAIKUTUS ENNUSTEESEEN

Turun yliopisto, Lääketieteellinen tiedekunta, Kliininen fysiologia ja isotooppilääketiede, Turun yliopiston kliininen tohtoriohjelma, Valtakunnallinen PET-keskus, Turun yliopistollinen keskussairaala, Turku, Suomi

Glioomat ovat pahanlaatuisia aivokasvaimia, joilla on taipumus uusiutua nopeasti. Kudosnäytteistä määritettävät molekyylipatologiset merkkiaineet ovat tärkeitä glioomien luokittelussa sekä ennusteen ja hoitovasteen arvioinnissa. Huonon ennusteen vuoksi glioomien uusia hoitomenetelmiä tutkitaan intensiivisesti.

Tämän väitöskirjatyön tarkoituksena oli tutkia somatostatiinireseptorien (alatyyppi 2, SSTR2) ilmentymistä glioomissa sekä histologian että positroniemissiotomografia/tietokonetomografiakuvauksen (PET/TT) avulla. Taustalla oli ajatus SSTR2:een sitoutuvasta radiolääkkeestä, jota on ehdotettu uusiutuneiden pahanlaatuisten glioomien hoitomuodoksi. Hoidon edellytyksenä on, että kasvaimet ilmentävät SSTR2:a, johon sekä PET-merkkiaine että radiolääke pääsevät sitoutumaan. Lisäksi tavoitteena oli potilaiden verinäytteistä tutkia mahdollisia biomerkkiaineita (GFAP, glial fibrillary acidic protein sekä EGFR, epidermal growth factor receptor) glioomien luokittelua ja seurantaa varten.

SSTR2:n ilmentymistä ja PET/TT-kuvantamista tutkittiin sekä kokeellisessa eläinmallissa että 27 potilaalla, jotka sairastivat pahanlaatuista glioomaa. Potilaiden verinäytteistä määritettiin lisäksi GFAP- sekä EGFR–pitoisuudet. Lopuksi SSTR2:n ilmentymistä tutkittiin retrospektiivisesti 184 glioomanäytteestä sekä ilmentymisen yhteyttä potilaan ennusteeseen.

Kokeellinen glioma ilmensi SSTR2:a, mutta PET/TT-kuvauksen hyöty tämän arvioimiseksi jäi alhaiseksi. Glioomapotilailla ei myöskään löytynyt yhteyttä kudosnäytteen SSTR2:n ilmenemisen ja PET-merkkiainekertymän välillä. Sen sijaan SSTR2:n ilmeneminen näytti liittyvän vahvasti aivokasvainten oligodendrogliaaliseen alatyyppiin sekä suotuisampaan ennusteeseen. Tämä yhteys vahvistettiin retrospektiivisessä työssä. Korkean seerumin GFAP-pitoisuuden todettiin lisäksi liittyvän aggressiivisiin glioblastoomiin sekä kasvaimen kokoon. Seerumin EGFR-pitoisuus sen sijaan ei liittynyt kasvainkudoksesta tehtyihin EGFR-määrityksiin.

Tulokset viittaavat siihen, että SSTR2 ja seerumin GFAP voivat toimia sekä luokittelevina että ennusteellisina biomerkkiaineina glioomien hoidossa ja/tai seurannassa. PET/TT-kuvantamisella on kuitenkin vähäinen merkitys radiolääkehoidon arvioinnissa.

Avainsanat: Gliooma, somatostatiinireseptori, PET, seerumin GFAP, oligodendroglioma

TABLE OF CONTENTS

ABBREVIATIONS

ATRX	Alpha-thalassemia/mental retardation syndrome X-linked
BBB	Blood-brain barrier
BP	Binding potential
CR	Coefficient of repeatability
CSF	Cerebrospinal fluid
DC	Dice similarity coefficient
DNA	Deoxyribonucleic acid
DOTA	1,4,7,10-Tetraazacyclodecane-1,4,7,10-tetraacetic acid
DOTANOC	DOTA-1Nal^3-Octreotide
DOTATATE	DOTA-Tyr^3-Octreotate
DOTATOC	DOTA-Tyr^3-Octreotide
DVR	Distribution volume ratio
EGFR	Epidermal growth factor receptor
ELISA	Enzyme-linked immunosorbent assay
FDG	Fluorodeoxyglucose
FDOPA	Fluoro-L-phenylalanine
FDR	Fluorodeoxyribose
FET	Fluoroethyl-L-thyrosine
FLAIR	Fluid-attenuated inversion recovery
GFAP	Glial fibrillary acidic protein
H&E	Hematoxylin and eosin staining
HGG	High-grade glioma (grades III and IV)
HPLC	High-performance liquid chromatography
ICC	Intraclass correlation coefficient
IDH	Isocitrate dehydrogenase
IHC	Immunohistochemistry
KPS	Karnofsky performance scale
MET	Methionine
MGMT	O6-methylguanine-DNA-methyltransferase
MRI	Magnetic resonance imaging
MRI-T1-Gad	Post-contrast T1-weighted MR images
mRNA	Messenger ribonucleic acid
NET	Neuroendocrine tumor
NOS	Not otherwise specified
OS	Overall survival
PCV	Procarbazine, CCNU (lomustine), and vincristine
PET/CT	Positron emission tomography/computed tomography
PFS	Progression-free survival
ROI	Region of interest
RT	Radiotherapy

RT-PCR	Reverse transcription polymerase chain reaction
SD	Standard deviation
SPECT	Single-photon emission computed tomography
SSTR	Somatostatin receptor (subtypes SSTR1, 2A, 2B, 3, 4, and 5)
SUV	Standardized uptake value
TAC	Time-activity curve
TMA	Tissue microarray
TMZ	Temozolomide
VOI	Volume of interest
V_{PET}	Tumor volume in PET
$V_{T1\text{-}Gad}$	Contrast-enhancing tumor volume in T1-weighted MR images
WHO	World Health Organization
1p/19q codeletion	Combined loss of chromosomal arms 1p and 19q
^{11}C	Carbon-11
^{111}In	Indium-111
^{177}Lu	Lutetium-177
^{18}F	Fluorine-18
^{68}Ga	Gallium-68
^{90}Y	Yttrium-90

LIST OF ORIGINAL PUBLICATIONS

1. Kiviniemi A, Gardberg M, Autio A, Li XG, Heuser VD, Liljenbäck H, Käkelä M, Sipilä H, Kurkipuro J, Ylä-Herttuala S, Knuuti J, Minn H, Roivainen A. Feasibility of experimental BT4C glioma models for somatostatin receptor 2-targeted therapies. Acta Oncol. 53(8):1125-1134, 2014.

2. Kiviniemi A, Gardberg M, Frantzén J, Pesola M, Vuorinen V, Parkkola R, Tolvanen T, Suilamo S, Johansson J, Luoto P, Kemppainen J, Roivainen A, Minn H. Somatostatin receptor subtype 2 in high-grade gliomas: PET/CT with ^{68}Ga-DOTA-peptides, correlation to prognostic markers, and implications for targeted radiotherapy. EJNMMI Res. Apr 22;5:25, 2015.

3. Kiviniemi A, Gardberg M, Frantzén J, Parkkola R, Vuorinen V, Pesola M, Minn H. Serum levels of GFAP and EGFR in primary and recurrent high-grade gliomas: correlation to tumor volume, molecular markers, and progression-free survival. J Neurooncol. 124(2):237-45, 2015.

4. Kiviniemi A, Gardberg M, Kivinen K, Posti JP, Vuorinen V, Sipilä J, Rahi M, Sankinen M, Minn H. Somatostatin receptor 2A in gliomas: association with oligodendrogliomas and favourable outcome. Accepted for publication in Oncotarget, 2017.

1 INTRODUCTION

Gliomas are diffusely infiltrating brain tumors classified as astrocytomas or oligodendrogliomas based on the cell of origin. Adult gliomas are graded as II, III, or IV with increasing aggressiveness. These traditional diagnostic principles have been integrated in the new 2016 World Health Organization (WHO) classification with molecular markers, which more accurately predict the patient outcome.

WHO classification guides therapeutic decision-making and emphasizes the importance of molecular biomarkers in gliomas. In addition to diagnostic guidance, biomarkers may provide information on the patient outcome (prognostic biomarker) or predict the response to certain therapies (predictive biomarker). The most powerful diagnostic and prognostic biomarker in gliomas today is isocitrate dehydrogenase (*IDH*) mutation. Biomarkers in the WHO classification are based on the analysis of biopsied tumor tissue. However, there has been increasing interest in "liquid biopsies," which use blood samples to allow for minimally invasive diagnoses and follow-up.

Due to diffuse infiltration, glioma recurrence is a rule rather than an exception, despite the optimal standard of care. Therefore, new treatment strategies in glioma management have been intensively studied. Pilot studies have reported beneficial responses to radionuclide therapy targeting somatostatin receptor subtype 2 (SSTR2) in gliomas. A method to detect *in vivo* SSTR2 expression in gliomas, however, is required to select patients who are likely to benefit from this demanding procedure. Furthermore, SSTR2 expression in gliomas is still controversial with conflicting results.

We aimed to examine SSTR2 expression with *in vivo* positron emission tomography (PET) imaging in rat and mice gliomas in an attempt to provide an experimental model for treatment strategies targeting SSTR2. A prospective clinical study was conducted to evaluate the ability of PET/computed tomography (CT) using tracers that bind to SSTR2 to detect high-grade glioma patients with high receptor density suitable for radionuclide therapy. Of particular interest was the association between SSTR2 expression, the oligodendroglioma component, and a favorable outcome, which led us to more extensively characterize SSTR2 expression and assess its diagnostic and prognostic values in a retrospective study including 184 glioma samples. Furthermore, serum levels of glial fibrillary acidic protein (GFAP) and epidermal growth factor receptor (EGFR) were studied as potential liquid biomarkers.

We hypothesized that SSTR2 and serum GFAP and EGFR may provide diagnostic, prognostic, and/or predictive value in gliomas.

2 REVIEW OF THE LITERATURE

2.1 General characteristics and epidemiology of gliomas

Gliomas are brain tumors originating from glial cells that support and surround the neural cells of the brain. They are designated as astrocytomas or oligodendrogliomas, depending on the cell of origin. Traditionally, they have been classified into highly aggressive WHO grade IV glioblastomas, anaplastic WHO grade III gliomas, or diffuse WHO grade II gliomas, indicating their growth potential and aggressiveness (Louis et al. 2007).

In the US, gliomas account for approximately 27% of all primary brain tumors and 80% of malignant primary brain tumors (Ostrom et al. 2015). The annual age-adjusted incidence of gliomas is about 50 new tumors per one million people, equating to almost 300 new gliomas in Finland (population 5.5 million) per year (Focus Oncologiae 2011). Although gliomas are rare, they are a significant cause of morbidity and mortality since the most frequent glioma, the WHO grade IV glioblastoma, is also the most aggressive, with a median survival of only 15 months (Stupp et al. 2005). In contrast, grade II gliomas are slow-growing, and despite their intrinsic tendency to progress over time to grades III or IV, they carry a better prognosis, with a median survival of up to 12 years (Okamoto et al. 2004).

2.2 Initial evaluation and treatment of gliomas

Glioma symptoms vary depending on the brain area affected, and may include seizures, motor and sensory weakness, mental status changes, problems with speech, headache, and nausea. Brain magnetic resonance imaging (MRI) is the modality of choice for initial evaluation and differential diagnosis when a brain tumor is suspected. Gliomas typically present as space-occupying lesions with peritumoral edema. High-grade gliomas (HGG, WHO grades III and IV) with an interrupted blood-brain barrier (BBB) commonly show enhancement after contrast administration, whereas low-grade gliomas (WHO grade II) usually do not. However, substantial overlap exists in the enhancement pattern, and consequently, a third of non-enhancing gliomas in adults are actually high-grade (Henson, Gaviani, and Gonzalez 2005).

In addition to conventional MRI (T1 pre- and post-contrast, T2, and FLAIR, i.e., fluid attenuation inversion recovery) and the structural information it provides, there are several advanced MRI techniques in clinical use nowadays that play a major role in diagnosis, grading, prognosis, surgical planning,

and assessment of treatment response in gliomas: MR perfusion, diffusion-weighted imaging (DWI), MR spectroscopy (MRS), diffusion-tensor imaging (DTI), and functional MRI (fMRI) are among the most important ones (Mohammadzadeh et al. 2016). MR perfusion estimates tumor vascularity and angiogenesis, where higher perfusion values indicate higher malignancy (Sadeghi et al. 2008). In contrast, DWI reflects the random microscopic motion of water molecules, which is restricted in tumor areas of increased cellularity, indicating a higher grade (Higano et al. 2006). MRS detects tissue metabolites, which are unique in gliomas compared to a normal brain. DTI and fMRI are especially used in surgical planning (Tieleman et al. 2009). DTI provides a three-dimensional view of the white matter tracts and their relationship to the tumor, which guides the neurosurgeon to reduce the risk of injury to critical tracts. In contrast, fMRI is used to localize sensory and motor cortices and essential language areas to allow for maximal tumor resection while preserving essential brain functions. The fMRI is based on blood oxygenation level dependent (BOLD) imaging, which measures neuronal activity indirectly while the patient is performing a task.

The multimodal management of gliomas begins with surgical resection whenever possible, while preserving neighboring eloquent brain areas. In glioblastomas, the maximal safe surgical resection is followed by radiotherapy and chemotherapy with temozolomide given both concomitantly and as an adjuvant treatment after radiotherapy (Stupp et al. 2005). General recommendations for the postoperative therapy of anaplastic and diffuse gliomas also include radiotherapy and/or chemotherapy, but especially in diffuse gliomas, the treatment guidelines are not as straightforward. Chemotherapy with PCV (procarbazine, CCNU, i.e., lomustine and vincristine) or temozolomide is favored in oligodendroglial tumors with 1p/19q codeletion. However, to date it is not clear which agent and combination with radiotherapy is optimal or whether radiotherapy could be deferred in 1p/19q codeleted tumors (Soffietti et al. 2010; Weller et al. 2014).

Treatment planning in gliomas is increasingly being based on certain molecular markers, such as 1p/19q codeletion in oligodendrogliomas, which predict better responses to chemotherapeutic agents. The promoter methylation of the DNA repair enzyme O^6-methylguanine-DNA-methyltransferase (MGMT) is related to the beneficial response to temozolomide and now guides the treatment decision in elderly glioblastoma patients who receive radiotherapy only if the tumor shows no *MGMT* methylation (Hegi et al. 2005; Weller et al. 2014).

Despite multimodality treatment, however, tumor recurrence is also the norm in low-grade gliomas. This limited response to standard therapies is

believed to result mostly from the diffuse infiltration of the tumor cells into the surrounding brain, which shelters them from surgery, radiation, and chemotherapy in case the blood-brain barrier (BBB) is intact (Cuddapah et al. 2014).

2.3 New 2016 WHO glioma classification

Gliomas have traditionally been classified according to their histology into astrocytomas, oligodendrogliomas, and oligoastrocytomas based on the assumed cell of origin. Additionally, the WHO classification of adult gliomas has assigned grades II–IV with respect to the grade of malignancy (Louis et al. 2007). Grade II gliomas are encountered in younger patients and regarded as low-grade, despite their substantial risk for malignant transformation over time, whereas grades III–IV are denoted as malignant or high-grade gliomas. The last decade, however, has witnessed expanding knowledge on the molecular basis of gliomas, discriminating glioma entities that predict patient outcome better than histological classification (Hartmann et al. 2010; Reuss et al. 2015). The discovery of mutations in the gene encoding isocitrate dehydrogenase-1 (*IDH1*) in a glioblastoma genome-wide sequencing study in 2008 was an especially significant landmark, and was followed by several studies identifying frequent *IDH1* mutation in gliomas at grades II and III, with incidences of up to 80% (Kloosterhof et al. 2011; Parsons et al. 2008). These advances have been acknowledged with the new 2016 revision of the WHO classification of tumors of the central nervous system, which combines histological and molecular features for an integrated classification (Louis et al. 2016). Major glioma entities are now distinguished by their IDH1 (or less commonly, IDH2) status, as well as the combined loss of the chromosomal arms 1p and 19q (1p/19q codeletion), as demonstrated in the diagnostic flow chart in Figure 1. The 1p/19q codeletion accompanying *IDH* mutation is the defining feature of oligodendrogliomas, therefore eliminating the diagnosis of mixed oligoastrocytomas by segregating them into oligodendrogliomas or astrocytomas if 1p/19q is intact. Histological tumor type and WHO grading are retained in the new classification, however, in case of discrepancy between the molecular and histological features, it is the genotype that rules over histology.

2.4 Diagnostic, prognostic, and predictive values of molecular markers

Molecular markers may be used as biomarkers to diagnostically help the pathologist in classifying the tumor (diagnostic biomarker), to evaluate the patient outcome (prognostic biomarker), or to predict the response to certain

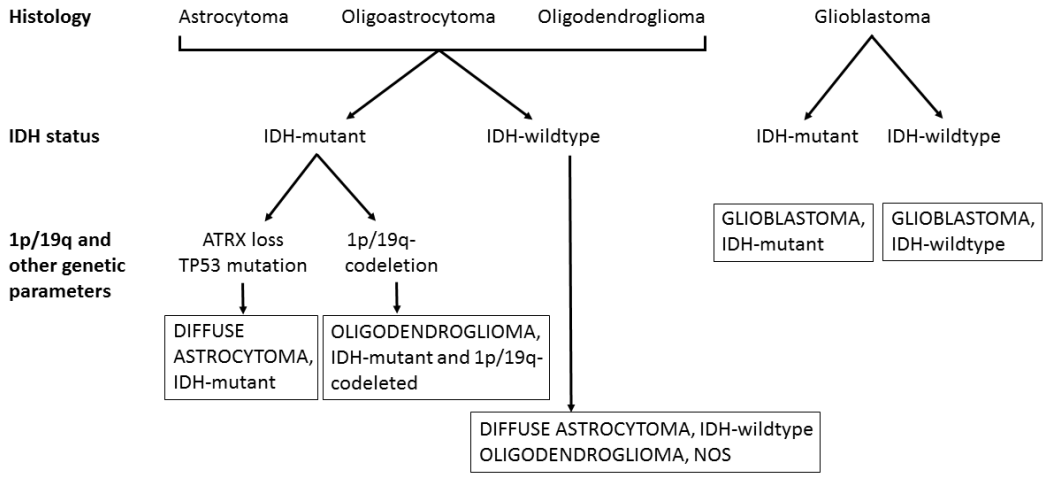

Figure 1. A simplified algorithm for the updated 2016 WHO classification of gliomas based on histological and genetic features. ATRX loss and TP53 mutation are characteristic but not required for diagnosis. Modified from Louis DN et al. (2016) Acta Neuropathol 131:803–820.

therapies (predictive biomarker). Most powerful and clinically significant biomarkers in gliomas are *IDH* mutation, 1p/19q codeletion, alpha-thalassemia/mental retardation syndrome X-linked (*ATRX*) mutation, and *MGMT* methylation, which are all assessed from tissue specimens.

2.4.1 Tissue biomarkers

Patients with *IDH*-mutated gliomas have beneficial outcomes compared to their wildtype counterparts. This benefit can even be seen across different WHO grades since patients with *IDH*-mutant glioblastomas have substantially improved survival times compared to patients with *IDH*-wildtype anaplastic astrocytomas (Hartmann et al. 2010). Furthermore, grades II and III *IDH*-mutant astrocytomas have similar overall survival rates, emphasizing the superior prognostic accuracy with IDH status compared to histology alone (Reuss et al. 2015).

The codeletion of 1p/19q is a highly relevant biomarker with diagnostic, prognostic, and predictive values. The 1p/19q codeletion characterizes oligodendroglial tumors and is associated with beneficial outcomes (Gorlia et al. 2013). Furthermore, 1p/19q codeletion predicts a superior response to chemotherapy (Cairncross et al. 2013; van den Bent et al. 2013).

Mutation and subsequent loss of ATRX expression is characteristic for *IDH*-mutant astrocytomas and is almost mutually exclusive with 1p/19q codeletion (Wiestler et al. 2013). Loss of ATRX expression has a role in tumor cells in

maintaining the length of telomeres, a region of repetitive DNA at each end of the chromosome (Heaphy et al. 2011). *IDH*-mutant astrocytomas with ATRX loss have better prognoses compared to *IDH*-mutant astrocytomas with retained ATRX expression (Wiestler et al. 2013). The definition of ATRX status is included in the new WHO classification, but is not mandatory for diagnosis.

As noted earlier, promoter methylation of the *MGMT* gene is a strong predictor of a beneficial response to alkylating chemotherapy (i.e., temozolomide) in newly diagnosed glioblastomas (Hegi et al. 2005). This is particularly relevant for treatment planning for elderly glioblastoma patients who usually have decreased tolerance for aggressive multimodality treatment. Therefore, monotherapy with temozolomide for patients whose tumors show *MGMT* promoter methylation and radiotherapy alone for patients whose tumors lack *MGMT* promoter methylation is justified nowadays in the clinical practice (Weller et al. 2014). Retrospective studies have also implicated a potential prognostic value of *MGMT* promoter methylation in *IDH*-mutant anaplastic astrocytomas (Wick et al. 2013). However, because MGMT promoter status is not known to be a diagnostic criterion for subtyping gliomas, it was not included in the new diagnostic WHO classification.

2.4.2 Liquid biomarkers

Established molecular diagnostics in gliomas, including *IDH* mutation and 1p/19q codeletion, are based on the analysis of biopsied or surgically resected tumor tissue. However, glioblastomas in particular are known to present significant intratumor heterogeneity with areas of different genetic alterations within the same tumor (Sottoriva et al. 2013). Consequently, molecular diagnostics from tumor tissue may be hampered by sampling error. Moreover, serial invasive tumor biopsies in the longitudinal monitoring of treatment response are not feasible. To solve this problem, advanced MRI techniques visualizing the whole tumor (perfusion and diffusion imaging) and "liquid biopsies" have been increasingly studied to allow for a minimally invasive diagnosis and follow-up of the heterogeneous tumor entity (Best et al. 2015; ElBanan et al. 2015).

Liquid biopsy is based on the biomolecules (proteins and nucleic acids) that a tumor cell or surrounding microenvironment release into circulation. Plasma and serum are routinely obtained from a peripheral venous blood sample, and are the most studied source of liquid biomarkers. Additionally, extracellular vesicles, platelets, or even complete circulating tumor cells can be extracted from collected blood and used to detect tumor-derived biomolecules (Best et

al. 2015). In gliomas, biomarkers can also be isolated from cerebrospinal fluid (CSF) surrounding the brain. However, collecting CSF is more invasive and carries potential risks compared to routine peripheral blood sampling.

2.4.2.1 Serum GFAP and EGFR

Glial fibrillary acidic protein (GFAP) is an intermediate filament expressed almost exclusively in astrocytes, where it acts as a member of the cytoskeleton. Serum levels of GFAP are known to be elevated after stroke and traumatic brain injury (Herrmann et al. 2000; Vos et al. 2010). Increased levels of circulating GFAP have also been detected in primary grade III and grade IV gliomas, suggesting a potential diagnostic value (Brommeland et al. 2007; Husain et al. 2012; Jung et al. 2007). In contrast, patients with metastatic brain lesion and healthy controls have not shown elevated serum GFAP, which may provide complementary data in the differential diagnosis of metastasis versus primary brain tumor (Jung et al. 2007). However, the prognostic value of circulating GFAP or its association with tumor burden in recurrent gliomas has not previously been studied.

Amplification of the epidermal growth factor receptor (*EGFR*) gene resulting in overexpression of EGFR is a hallmark of primary glioblastomas and is associated with low rates of survival (Ohgaki and Kleihues 2007; Shinojima et al. 2003). *EGFR* amplification is detected in approximately 40% of *de novo* glioblastomas, and half of these additionally demonstrate *EGFRvIII* mutation, rendering EGFR and EGFRvIII attractive targets for therapy and raising the need for a circulating biomarker for treatment monitoring (Hegi, Rajakannu, and Weller 2012). Elevated levels of serum EGFR have been detected in patients with glioblastomas compared to anaplastic astrocytomas and healthy controls (Quaranta et al. 2007). However, the prognostic value or the association between serum and tumor tissue EGFR status has not been studied.

2.5 Somatostatin receptors

Somatostatin receptors (SSTR) are a family of G protein-coupled transmembrane receptors consisting of five different subtypes (SSTR1–5). In rodents, SSTR2 mRNA is further spliced, giving rise to two protein isoforms, SSTR2A and SSTR2B, which differ in length and composition of intracellular carboxy-termini (Vanetti et al. 1992). A 2.3 Kb transcript corresponding to SSTR2B has also been identified in human tissue, suggesting that alternative splicing exists in human SSTR2 mRNA (Patel et al. 1993).

SSTRs are differentially distributed throughout the central nervous system and peripheral tissues, where they mediate the neuronal and hormonal effects of somatostatin. SSTR2 is considered the most abundant subtype in the brain, where it is expressed in neurons and neuropil, especially in the cortex, amygdala, and hippocampus (Cole and Schindler 2000; Videau et al. 2003). Somatostatin plays a key role in the control of pituitary hormone release, providing a therapeutic target for long-acting somatostatin analogs such as octreotide and lanreotide, which are used in the treatment of acromegaly for inhibiting growth hormone secretion (Lamberts et al. 1996). Furthermore, in the central nervous system, somatostatin acts as a neuromodulatory agent, mediating various motor, cognitive, and sensory effects (Viollet et al. 2008). Interestingly, reduced somatostatin levels and deficits in SSTR2 expression have been associated with neuropsychiatric and neurodegenerative disorders, such as major depression and Alzheimer's disease, respectively, with potential therapeutic targeting (Adori et al. 2015; Lin and Sibille 2013).

2.5.1 Somatostatin receptors in human cancer

SSTRs have been identified in various solid tumors with the most notable expression in neuroendocrine tumors (NETs), neuroblastomas, meningiomas, and lymphomas (Reubi et al. 1992). SSTR expression is usually related to tumor differentiation with well-differentiated NETs expressing SSTR in the majority of cases, whereas the less differentiated NETs often lack SSTR (Theodoropoulou and Stalla 2013).

Somatostatin analogs predominantly targeting SSTR2 have the potential to block tumor growth via direct and indirect mechanisms. The antiproliferative action is mediated by inhibiting the effects of growth factors and downregulating their synthesis by blocking the tumor cell cycle progression, inducting apoptosis, and inhibiting angiogenesis (Theodoropoulou and Stalla 2013). Furthermore, SSTR2 itself is considered to be a tumor suppressor, demonstrating a significant reduction of pancreatic tumor growth after adenoviral vector-based SSTR2 gene transfer in a pancreatic cancer model (Vernejoul et al. 2002). In clinical practice, somatostatin analogs are used in NETs for supportive care to alleviate the hypersecretion-related symptoms in patients with the carcinoid syndrome, but also as an option to stabilize the tumor growth (Eriksson et al. 2008).

2.5.2 SSTR2-targeted radiotherapy in cancer

Radionuclide therapy targeting SSTR2 employs somatostatin analogs that are radiolabeled with β^--emitting isotopes. The most commonly used derivatized somatostatin analogs are DOTA-Tyr^3-Octreotide (DOTATOC) and DOTA-Tyr^3-Octreotate (DOTATATE), which have the highest affinity for SSTR subtype 2 (Reubi et al. 2000). The β^--emitting isotopes mediating the targeted radiation therapy include Yttrium-90 (^{90}Y) and Lutetium-177 (^{177}Lu). Both ^{90}Y-DOTATOC and ^{177}Lu-DOTATATE are widely used in clinical practice to target metastatic or inoperable NETs abundantly expressing SSTR2 and leading to partial or complete objective responses in up to 30% of NET patients (Bodei et al. 2013). Diagnostic imaging with PET/CT using Gallium-68- (^{68}Ga) based peptides is used for staging and to identify tumors that overexpress SSTR2, predicting the response to targeted radionuclide therapy (Maecke and Reubi 2011). Encouraging results have also been reported for other SSTR2-positive tumors, including recurrent meningiomas and childhood neuroblastomas treated with ^{90}Y-DOTATOC or ^{177}Lu-DOTATATE (Bartolomei et al. 2009; Gains et al. 2011).

2.5.3 SSTR2-targeted radiotherapy in gliomas

Three pilot studies have investigated the role of SSTR2-targeted radionuclide therapy with ^{90}Y-DOTATOC in gliomas (Heute et al. 2010; Merlo et al. 1999; Schumacher et al. 2002). To circumvent BBB, ^{90}Y-DOTATOC was locoregionally delivered to the resection cavity or to the solid tumor in all cases presented. In general, radionuclide therapy was well tolerated. Eleven patients with a progressive glioma of grades II–IV were included in a study by Merlo et al. (1999). They found that a low activity-to-dose ratio (i.e., injected activity divided by the tumor dose) was related to a favorable treatment response (no progression on MRI and clinically stable for a progression-free survival period), and is indicative for high SSTR2 expression and specific binding of ^{90}Y-DOTATOC. A beneficial response was reported in 7 out of 11 gliomas, including one glioblastoma. In an extended pilot study including only grade II–III gliomas, Schumacher et al. also examined the applicability of locally injected ^{90}Y-DOTATOC in newly diagnosed low-grade gliomas and found this approach feasible for further trials (Schumacher et al. 2002). The most recent study included three patients with recurrent glioblastomas with a positive ^{68}Ga-DOTATOC PET/CT performed in one of the patients (Heute et al. 2010). Exceptionally encouraging results were reported with a complete remission in one patient, who was still alive four years after admission to the study, and partial response in the other two, who experienced only minor side effects. However, for a wider acceptance of this technically demanding

procedure, further clinical trials and a clear definition of the patients who are most likely to benefit from it are needed.

2.5.4 SSTR2 expression in gliomas

Studies on SSTR2 expression in gliomas have demonstrated controversial results. Reubi et al. concluded from their autoradiographic assays that SSTRs are expressed predominantly by low-grade and anaplastic gliomas, with 10 out of 12 astrocytomas and 2 out of 4 oligodendrogliomas showing SSTR expression, whereas only 1 out of 20 glioblastomas showed binding of the radiolabeled somatostatin analog *in vitro* (Reubi et al. 1987). Similar results with low SSTR2 expression in glioblastomas were reported in another study using reverse transcription polymerase chain reaction (RT-PCR), immunohistochemistry (IHC), and autoradiography (Cervera et al. 2002). In oligodendrogliomas, however, the tumors were mostly SSTR2-negative in autoradiography, despite high mRNA by RT-PCR (Cervera et al. 2002). In contrast, others have reported opposite results by showing SSTR expression mainly in high-grade gliomas. In a series of 8 diffuse astrocytomas, 10 anaplastic astrocytomas, and 32 glioblastomas, immunohistochemistry with polyclonal antibody demonstrated positive SSTR2A in 44% of glioblastomas, but in only 10% of anaplastic and 0% of diffuse astrocytomas (Mawrin et al. 2004). The authors concluded that the loss of differentiation in glioblastomas was associated with increased expression of SSTR1, SSTR2A, and SSTR3. No oligodendroglial tumors were included in this study. Dutour et al. reported expression of SSTR2 mRNA by Northern blot in 6 out of 9 gliomas, with the highest expression detected in one glioblastoma and two oligodendrogliomas (Dutour et al. 1998). In summary, several studies show variable results regarding SSTR2 expression in gliomas. A limited number of cases have been included in the studies, with 50 gliomas being the largest cohort of samples (Mawrin et al. 2004). The number of oligodendrogliomas included in the studies has been even further limited. A more systematic characterization of SSTR2 expression in gliomas is needed with emphasis on molecular profiling and SSTR2-targeted therapies readily available.

Since autoradiographic or Northern blot analyses are unable to define the exact location of SSTR2 expression, IHC with the ability to detect subcellular structures would be the preferred method. Until recently, however, the available antibodies for IHC have been polyclonal, which display heterogeneity from batch to batch and cross-reactivity with other antigens (Reubi et al. 1999). A monoclonal antibody (UMB-1) targeting the intracellular C-termini of SSTR2A was recently developed and is now commercially available, showing considerably more effective and cleaner

staining compared with polyclonal antisera (Fischer et al. 2008). IHC with UMB-1 has subsequently been widely studied and used, and is now the recommended method of choice for SSTR2A detection (Korner et al. 2012).

2.6 Positron Emission Tomography

Positron Emission Tomography (PET) allows the visualization and quantification of different biochemical processes *in vivo*. PET uses radioactive tracers that accumulate to areas such as increased metabolic activity or cell proliferation, or that act as specific agents that bind to tumor-specific receptors or antigens.

The procedure of PET imaging is depicted in Figure 2. After labelling with a positron-emitting isotope (e.g., ^{18}F, ^{11}C, or ^{68}Ga), the radioactive tracer is

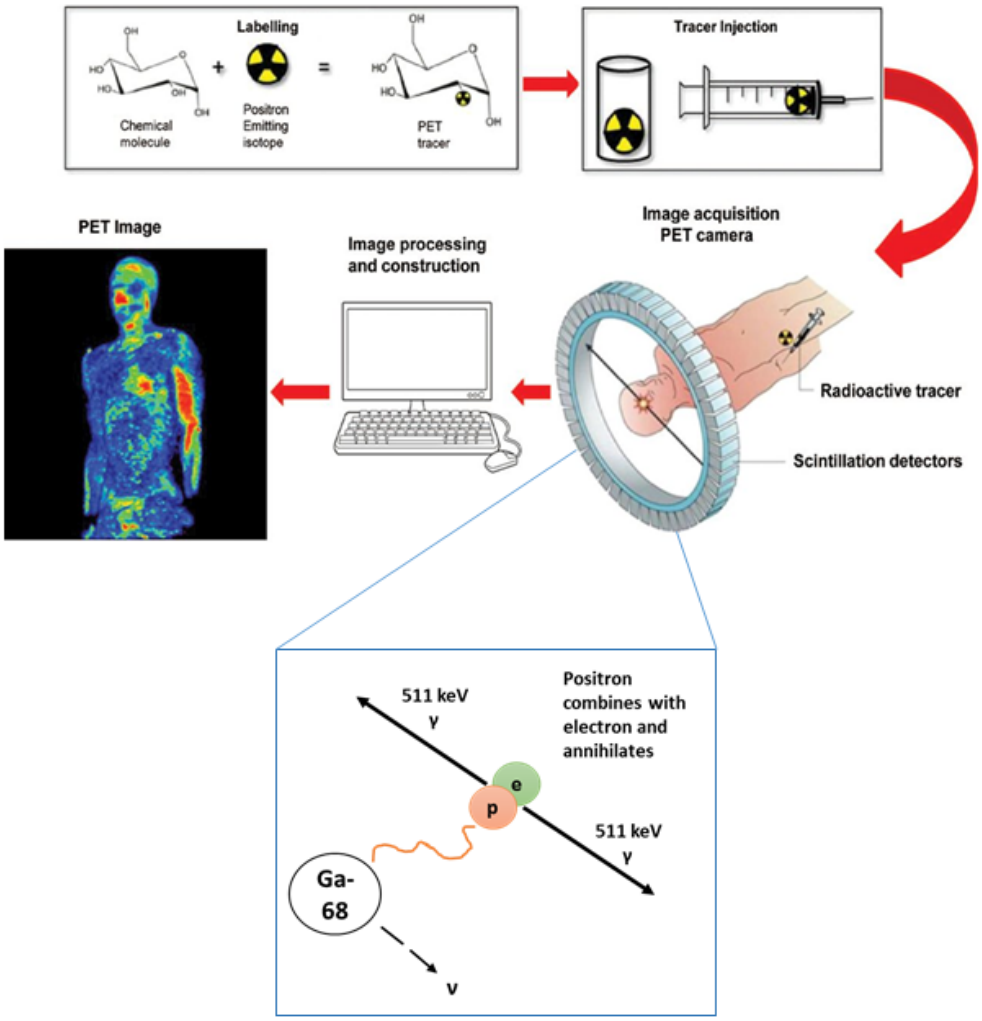

Figure 2. Procedure of PET imaging. Modified from Rudroff et al. (2015) J Appl Physiol 118:1181–1190.

intravenously injected into the patient, where it accumulates in its target tissue. The isotope decays by releasing a positron, which traverses a very short distance in the tissue (range) before it combines (annihilates) with an electron. In the process of annihilation, a pair of 511 keV photons are emitted in opposite directions, where the coincident photons are detected by the scintillation crystals in the PET scanner (Basu et al. 2011).

Most of the PET scanners are now hybrid devices in which PET and computed tomography (CT) are fused together. CT adds two important features: first, it allows for more accurate anatomic location, and second, it helps to correct the attenuation of the photons due to their energy loss in the body. Several additional corrections are made, including for random and scattered coincidences. To obtain a diagnostic image, the raw data must be further reconstructed. Several algorithms are possible, but the iterative reconstruction methods have largely become the standard approach (Mittra and Quon 2009). PET images typically have worse spatial resolution compared to CT and magnetic resonance (MR) images. This is mostly related to fundamental limitations, including the detector size, positron range, and noncollinearity of the annihilated photons (Basu et al. 2011). However, PET enables molecular and functional imaging that are not available with MRI or CT at the moment.

Tracer uptake can be semiquantitatively analyzed by calculating a Standardized Uptake Value (SUV), which depends on the radioactivity concentration measured by the PET scanner within a region of interest, the decay-corrected amount of injected radiolabeled tracer, and the weight of the patient.

2.6.1 Clinical PET imaging in gliomas

The most common PET tracer for oncologic imaging has traditionally been ^{18}F-fluorodeoxyglucose (^{18}F-FDG), which accumulates in the majority of tumors due to their increased glucose metabolism. However, the visualization of brain tumors with ^{18}F-FDG PET is poor due to the high physiological uptake by the normal brain tissue. Consequently, most commonly used PET tracers for gliomas in the clinical setting are amino acid tracers such as ^{11}C-methionine (^{11}C-MET), ^{18}F-fluoroethyl-L-tyrosine (^{18}F-FET), and ^{18}F-fluoro-L-phenylalanine (^{18}F-FDOPA), which have an increased uptake in gliomas due to elevated amino acid utilization in tumor cell proliferation (Galldiks, Langen, and Pope 2015). Amino acid PET provides additional information to standard MRI and may help in the clinical dilemmas of detecting tumor tissue when MRI is inconclusive, differentiating true glioma progression from postradiation treatment effects (pseudoprogression or radiation necrosis) and detecting progression in the non-enhancing tumor

after antiangiogenic treatment with a possible pseudoresponse in the contrast-enhancing tumor portion (Galldiks, Langen, and Pope 2015).

2.6.2 PET imaging of somatostatin receptors

Imaging SSTR-expressing tumors has been performed for several decades with conventional gamma camera scintigraphy and single-photon emission computed tomography (SPECT)/CT using octreotide as a tracer radiolabeled with Indium 111 (^{111}In). However, scintigraphy yields planar 2D images with rather poor spatial resolution and low sensitivity to detect small lesions. In addition, ^{111}In has a long physical half-life of 2.8 days, resulting in at least a 24-hour delay between the radiotracer injection and image acquisition (Virgolini et al. 2010). Accordingly, PET tracers labeled with Gallium 68 (^{68}Ga; physical half-life 68 min) have been developed to allow SSTR imaging with PET/CT, providing superior detail, speed, and lower radiation dose to the patient compared to SSTR scintigraphy (Virgolini et al. 2010).

PET/CT using ^{68}Ga-labeled somatostatin analogs is widely used in the clinical management of NETs to localize primary tumors, detect sites of metastasis or recurrent disease, and to determine SSTR status and select patients for SSTR-targeted radiotherapy (Hofman, Lau, and Hicks 2015; Loimaala et al. 2014). Three DOTA-chelated somatostatin analogs are available for clinical imaging: ^{68}Ga-DOTATOC, ^{68}Ga-DOTA-1NaI^{3}-octreotide (^{68}Ga-DOTANOC), and ^{68}Ga-DOTATATE. All three radiotracers have the highest affinity for SSTR2. ^{68}Ga-DOTATOC shows additional binding to SSTR5, and ^{68}Ga-DOTANOC to SSTR3 and SSTR5 (Reubi et al. 2000; Wild et al. 2003). ^{68}Ga-DOTATATE has a predominant affinity only for SSTR2 (Reubi et al. 2000). Only subtle differences between the tracers, however, has been observed in clinical utility (Kabasakal et al. 2012; Velikyan et al. 2014).

In neuroendocrine tumors, SUV in ^{68}Ga-DOTATOC PET/CT has been shown to correlate with SSTR2 expression determined by immunohistochemistry, whereas no association with SSTR3 or SSTR5 immunostaining was reported (Miederer et al. 2009; Mussig et al. 2010). A similar correlation between ^{68}Ga-DOTATOC uptake and SSTR2 mRNA analyzed by RT-PCR has been found in normal human tissue (Boy et al. 2011).

The benefit of PET/CT with ^{68}Ga-DOTA-peptides has been studied in a number of other tumors as well, including meningioma, neuroblastoma, and pheocromocytoma (Hofman, Lau, and Hicks 2015). In meningiomas known to overexpress SSTR2, ^{68}Ga-DOTATOC PET/CT potentially improves the tumor delineation for radiation treatment planning (Nyuyki et al. 2010). Furthermore,

increased pretreatment of ^{68}Ga-DOTA-peptide uptake is associated with beneficial response to SSTR2-targeted radionuclide therapy in progressive meningiomas after failure of standard treatment options (Seystahl et al. 2016).

2.6.3 SSTR PET in gliomas

SSTR imaging in gliomas was studied two decades ago with conventional scintigraphy using ^{111}In-DTPA-octreotide. These two studies showed that ^{111}In-DTPA-octreotide uptake was dependent on the integrity or disruption of the BBB (Haldemann et al. 1995; Schmidt et al. 1998). Haldemann et al. demonstrated positive SSTR scintigraphy in all six gliomas with disrupted BBB; however, only two (anaplastic oligodendroglioma and low-grade astrocytoma) presented SSTR expression in the *in vitro* autoradiography of the resected tumor, while no SSTR expression was observed in the other four glioblastomas. Conversely, false negative scintigraphy was noted in astrocytomas grades II–III with positive SSTR autoradiography but intact BBB (Haldemann et al. 1995). These results suggest a limited role for SSTR scintigraphy for tumor detection or delineation in gliomas with variable SSTR expression.

More recently, a pilot study including three recurrent glioblastomas treated with locoregional SSTR radionuclide therapy with ^{90}Y-DOTATOC demonstrated encouraging results, with a complete remission in one patient and partial remission in the other two with only minor side effects (Heute et al. 2010). ^{68}Ga-DOTATOC PET in the case of complete remission showed increased tracer uptake prior to therapy, which was normalized in follow-up scans. Since tumor SSTR2 expression is mandatory for successful therapy, we hypothesize that ^{68}Ga-DOTA-peptide PET/CT could provide a method to select patients likely to benefit from radionuclide therapy with ^{90}Y-DOTATOC. Moreover, in addition to the superior spatial resolution compared to scintigraphy, SSTR PET/CT enables dynamic kinetic analyses to quantify the target receptor occupancy. As reviewed and debated by Sharma et al., ^{68}Ga-DOTA-peptide PET/CT is unlikely to have a major role in glioma imaging with one exception. Radionuclide therapy with ^{90}Y-DOTATOC is the one condition where it is potentially useful by showing *in vivo* SSTR2 expression prior to therapy and providing proper patient selection (Sharma et al. 2013). To the best of our knowledge, there has not been any systematic assessment of ^{68}Ga-DOTA-peptide PET/CT in high-grade gliomas prior to our study.

2.7 Glioma animal models

Rat brain tumor models have been used extensively for several decades to assess the efficacy of innovative approaches for the treatment of brain tumors. The advantages of rat brain tumor models (as opposed to mouse models) are their longer survival and greater tumor size, permitting better *in vivo* imaging and larger amounts of therapeutic agents administered, to mention a few (Barth and Kaur 2009). However, the ability to produce genetically engineered and manipulated tumor cell lines has also increased the use of mouse models over the past decade (Kegelman et al. 2014).

The most popular rat brain tumor models are based on the syngeneic orthotopic approach, indicating reproducible tumors transplanted into the brain of a genetically similar host through stereotactic injection. A C6 glioma and 9L gliosarcoma have been widely used (Barth and Kaur 2009). However, their growth patterns are rather circumscribed in contrast to the infiltrative border typically seen in human gliomas. Also, the tumors are strongly immunogenic. In contrast, F98 and BT4C gliomas show an infiltrative growth pattern and weak immune response, mimicking the authentic human tumor (Barth and Kaur 2009). BT4C gliomas further demonstrate small necrotic areas, neovascularization, and high cellularity with marked pleomorphism and nuclear atypia typical for human high-grade gliomas.

SSTR2 has been studied as a potential therapeutic target in only a few glioma models. Barbieri et al. detected SSTR1-3 and SSTR5 mRNA in C6 glioma cells *in vitro*, where they mediated antiproliferative effects via inhibition of extracellular signal-regulated kinase (ERK)1/2 activity (Barbieri et al. 2008). Somatostatin and SSTR agonists also strongly inhibited tumor growth *in vivo* in nude mice xenografted with C6 glioma cells (Barbieri et al. 2009). Somatostatin acting on SSTR1, SSTR2, and SSTR5 showed the highest efficacy, although combined SSTR1 and SSTR2 agonists maximally reduced the tumor neovascularization. Another study using nude mice xenografted with DBTRG-05 glioblastoma cells showed that a somatostatin analog linked to a chemotherapeutic doxorubicin molecule significantly inhibited tumor growth compared to animals treated separately with equimolar doses of doxorubicin or somatostatin analog only (Pozsgai et al. 2010). Despite increasing interest in SSTR2-targeted therapies, there are no studies focusing on SSTR2 expression, targeting, and imaging in orthotopic syngeneic rat glioma models and providing the best available model simulating human high-grade glioma.

3 AIMS OF THE STUDY

The aim of this doctoral thesis was to study new potential biomarkers in gliomas with special emphasis on characterizing tissue SSTR2 expression and studying the potential of PET/CT to detect SSTR2 in gliomas that would benefit the procedure of SSTR2-targeted radionuclide therapy. More specific aims of each substudy were as follows:

I. To characterize SSTR2 expression in a rat orthotopic and mouse xenograft BT4C glioma model and to visualize the tumor *in vivo* with PET/CT using ^{68}Ga-DOTATOC and ^{18}F-FDR-NOC, a novel tracer targeting SSTR2.

II. To prospectively use PET/CT to evaluate the potential of ^{68}Ga-DOTANOC or ^{68}Ga-DOTATOC to target SSTR2 in primary or recurrent high-grade glioma, to *in vivo* detect patients suitable for SSTR2-targeted radionuclide therapy, and to examine the relationship between ^{68}Ga-DOTA-peptide uptake with BBB integrity and SSTR2 immunohistochemistry.

III. To prospectively study the serum levels of two potential liquid biomarkers, GFAP and EGFR, in patients with primary or recurrent high-grade glioma, and to examine their association with tumor burden in MRI, other prognostic molecular markers, and survival.

IV. To extensively characterize SSTR2 expression by immunohistochemistry and explore its impact on survival in a retrospective cohort of glioma entities using the specific molecular signatures of the updated 2016 WHO classification.

4 MATERIALS AND METHODS

4.1 BT4C cell line and animal models (I)

The BT4C rat glioma cell line was originally derived from fetal BDIX rat brain cells transferred to long-term culture after *in vivo* exposure to N-ethylnitrosurea (Laerum and Rajewsky 1975). Cells were grown in Dulbecco's modified Eagle medium (DMEM), supplemented with 10% fetal calf serum (Gibco, Paisley, Scotland), 2 mM glutamine, 2 mM sodium pyruvate, and 50 µg/mL streptomycin at 37° C in the presence of 5% CO_2.

Stereotactic injections of BT4C cells into the brain of nine male BDIX rats (Charles River, France, weighing 263–354 g) were performed as described earlier (Tyynelä et al. 2002). Briefly, rats were anesthetized intraperitoneally (i.p.) with ketamine and medetomidine and placed into stereotactic apparatus (Kopf Instruments, Tujunga, CA, USA). A total of 10,000 BT4C cells in 5 µL of Optimem medium were slowly injected with a 25 µL Hamilton syringe 27 G needle (Hamilton, Bonaduz, Switzerland) into the right corpus callosum (coordinates: 1.0 mm caudal to bregma and 2.0 mm right to sutura sagittalis at a depth of 2.5 mm). The needle was left in place for 5 min before removal to avoid backflow. The presence of a tumor was verified by an MRI T2-weighted spin-echo sequence using a 4.7 T magnet (Magnex, Abington, UK) 13 days after the BT4C cell injection. For the subcutaneous tumor model, 16 male athymic nude mice (Harlan) were kept under isoflurane anesthesia while 250,000 BT4C cells in 100 µL of Matrigel (Matrigel Matrix, BD Biosciences) were injected subcutaneously into the neck and left limb of each mouse.

4.2 Preparation of radiotracers (I, II)

^{68}Ga was obtained from a ^{68}Ge/^{68}Ga generator (Eckert & Ziegler, Berlin, Germany). For the radiosynthesis of ^{68}Ga-DOTATOC and ^{68}Ga-DOTANOC, a fully automated synthesis device was used (Modular Lab, Eckert & Ziegler Eurotope GmbH, Berlin, Germany) as previously described (Belosi et al. 2013). In animal studies, the radiochemical purity of ^{68}Ga-DOTATOC exceeded 99%, and the specific radioactivity was 18 GBq/µmol (median). In human studies, the corresponding values for ^{68}Ga-DOTATOC were 97% and 27 GBq/µmol, and for ^{68}Ga-DOTANOC 100% and 32 GBq/µmol, respectively. The novel tracer ^{18}F-FDR-NOC in study I was prepared by conjugating the ^{18}F-fluorodeoxyribose as a prosthetic group to the somatostatin analog NOC peptide (Rinne et al. 2016). The radiochemical purity of ^{18}F-FDR-NOC was

99% and specific activity 33 GBq/μmol. Corresponding measurements for ^{18}F-FDG were > 95% and 0.3–1 TBq/μmol.

4.3 SSTR2 PET/CT in animal models (I)

A dedicated small animal PET/CT scanner with an axial FOV of 12.5 cm was used (Inveon Multimodality PET/CT, Siemens Medical Solutions, Knoxville, TN, USA). All nine rats and eight mice were studied with ^{68}Ga-DOTATOC, and an additional eight mice with ^{18}F-FDR-NOC prior to *ex vivo* biodistribution and autoradiography measurements. PET/CT was performed 23–25 days after stereotactic and 26–30 days after subcutaneous BT4C injections. A 60-min dynamic acquisition consisting of 38 time frames (12 × 5 s; 12 × 30 s; 8 × 60 s; 3 × 300 s; and 3 × 600 s) started at the time of injection via a tail vein catheter (^{68}Ga-DOTATOC rats 30.8 ± 3.2 MBq and mice 11.6 ± 2.1 MBq; ^{18}F-FDR-NOC 13.5 ± 1.1 MBq). Animals were anesthetized with isoflurane and kept on a warm pallet during the imaging procedure. A static 20-min ^{18}F-FDG PET/CT starting 45 min after injection (14.5 ± 0.4 MBq) was performed on eight mice undergoing ^{18}F-FDR-NOC PET/CT on the previous day. A CT was used for attenuation correction, and PET images were iteratively reconstructed using a two-dimensional ordered subsets expectation maximization algorithm (OSEM2D, 4 iterations, 16 subsets) and a 128 × 128 × 159 matrix size.

4.3.1 PET analysis in animal models

Analyses were performed using software developed in-house (Carimas 2.8; http://www.turkupetcentre.fi/carimas/). Spherical volumes of interest (VOI) were defined on the tumor, normal brain, heart, liver, and kidney. The brain tumor was localized next to the cranial drill hole. Radioactivity concentrations were corrected for the injected dose, the radioactivity remaining in the tail, and decay. Results are presented as mean SUVmax for tumor and mean SUVaverage for other organs. Time-activity curves (TACs) were extracted from the corresponding dynamic images. Tumor uptake in ^{18}F-FDG PET/CT was reported as scaled SUV that takes into consideration the measured blood glucose levels.

4.3.2 *Ex vivo* biodistribution, radiotracer stability, and autoradiography

Animals were euthanized immediately after ^{68}Ga-DOTATOC or ^{18}F-FDR-NOC PET/CT. Radioactivity concentration in excised organs was measured

with a gamma counter (Triathler Gamma with external 3" NaI detector, Hidex Oy, Turku, Finland) to determine the *ex vivo* biodistribution of the radiotracer. Measured radioactivity was corrected for decay, weight of the organ and animal, and background radioactivity, and was expressed as SUV. Infiltrative brain tumors could not be separately measured with the gamma counter. The *in vivo* stability of ^{68}Ga-DOTATOC and ^{18}F-FDR-NOC at 60 min post-injection was measured from plasma by radio high-performance liquid chromatography (HPLC) analysis.

Autoradiography analysis was performed to determine tracer uptake in the tumor, brain, and muscle. After gamma counting, tissues were frozen and cut into serial 8- and 20 µm cryosections, with a cryomicrotome at -15° C thaw-mounted onto microscope slides and opposed to an imaging plate (Fuji Imaging Plate BAS-TR 2025, Fuji Photo Film Co., Ltd., Tokyo, Japan). After an exposure time of 2.5 h for ^{68}Ga-DOTATOC and 4 h for ^{18}F-FDR-NOC, the imaging plates were scanned with the Fuji Analyzer BAS-5000 (Fuji Photo Film Co., Ltd., Tokyo, Japan; internal resolution of 25 µm). Radioactivity of the tumor, brain, and muscle was measured from the 20 µm sections and expressed as photostimulated luminescence units per square millimeter (PSL/mm^2) using Tina 2.1 software (Raytest Isotopenmessgeräte GmbH, Straubenhardt, Germany). Circular ROIs were defined for the tumor in accordance with hematoxylin and eosin (H&E) staining from areas with the highest tumor cellularity. Several tissue sections were analyzed for each animal, and results are expressed as mean ± standard deviation (SD).

4.3.3 SSTR2A immunohistochemistry and Western blot analysis in animal models

SSTR2A immunostainings and H&E were performed on the 8 µm slides. Monoclonal antibody UMB-1 (Abcam, Cambridge, UK) was used for SSTR2A IHC employing a Ventana Benchmark XT or LabVision autostainer. Western blot analysis was performed on BT4C cells using rat adrenal gland, kidney, and spleen as positive controls.

4.4 Patient characteristics in the prospective study (II, III)

Thirty patients with radiologically suspected primary or recurrent HGG scheduled for tumor resection between 2011 and 2013 were prospectively enrolled (mean age 52 years; range 18–76 years). A ^{68}Ga-DOTA-peptide PET/CT was performed prior to surgical resection with a mean interval of 19 days. Two patients with final diagnoses of metastatic adenocarcinoma and malignant lymphoma were excluded from the final analyses. Additionally,

PET/CT was not performed on one patient due to a scheduling problem, but the tumor sample was included for SSTR2 IHC. Finally, 27 patients with primary (n=17) or recurrent (n=10) HGG underwent ^{68}Ga-DOTA-peptide PET/CT. Preoperative venous blood samples were obtained. Additionally, postoperative blood samples were collected 2–5 days after surgical resection in 20 of these patients. In study III, serum samples of 13 healthy subjects (mean age 54 years) without history of cancer or neurological symptoms were used as controls.

4.4.1 ^{68}Ga-DOTA-peptide PET/CT in patients with high-grade glioma (II)

PET/CT of the brain was performed using a GE Discovery VCT PET/CT Scanner (General Electric Medical Systems). Dynamic PET was acquired over 60 minutes (8 x 15; 6 x 30; 5 x 180; 4 x 300; and 2 x 600 s frames) after intravenously injected ^{68}Ga-DOTANOC (123 MBq, median) or ^{68}Ga-DOTATOC (130 MBq, median). ^{68}Ga-DOTATOC was used for the first three patients, after which it was replaced by ^{68}Ga-DOTANOC due to poor availability of the DOTATOC precursor. A low-dose CT (120 kV, 10–95 mA, noise index 25, slice thickness 3.75 mm) was used for attenuation correction. PET images were reconstructed (256x256 matrix, OSEM3D, three iterations, 28 subsets, 4.8 mm Hanning postfilter), yielding to a pixel size of 1.4 mm. A 60-min duration was determined after a 90-min dynamic PET was performed on one patient and 5-min static scans were performed on three patients 96 min post-injection, which confirmed that the tumor uptake did not increase after 60 min. One patient underwent a static PET scan (28 to 58 min post-injection) due to mild claustrophobia. Dynamic PET was discontinued in two patients at 53 min and 36 min post-injection due to dyspnea and numbness of the arm, respectively. Clinical preoperative MRI nearest in time to the PET scan (mean interval 14 days) was employed, and post-contrast T1-weighted images (MRI-T1-Gad) were used to define the tumor volume with contrast enhancement.

4.4.2 Quantitative PET analysis of high-grade gliomas (II)

Analyses were performed using software developed in-house (Carimas 2.7). PET and MRI-T1-Gad images were co-registered, and spherical volumes of interest (VOI) were manually placed over the tumor area with maximum activity. VOIs for contralateral normal brain white matter, nasal mucosa, pituitary gland, and skin of the occiput were also defined and SUVmax were calculated. Tumor mean SUVmax 30–60 min post-injection was used for further analyses.

A Logan plot with skin as reference tissue was used for tracer kinetic modeling. We used 5 min as the starting point for a linear regression model that was optimized against the normalized tumor and reference tissue TACs, with the slope being the distribution volume ratio (DVR). Binding potential (BP) corresponds to the density of available receptors and is calculated as BP = DVR – 1.

4.4.3 Delineation of tumor volumes in PET and MRI (II, III)

Tumor volumes were delineated using iPlan RT Treatment Planning software (Brainlab, Munich, Germany). PET and MRI images were coregistered and tumor volume contoured in PET using a threshold of 40% SUVmax (V_{PET}). Contrast-enhancing tumor volume in T1w MRI ($V_{T1\text{-}Gad}$) was delineated by thresholding the enhancing tumor and then manually adjusting the contours. To compare tumor volumes between PET and MRI, overlapping volumes of V_{PET} and $V_{T1\text{-}Gad}$ were determined and Dice similarity coefficient (DC = [2 x intersection]/[V_{PET} + $V_{T1\text{-}Gad}$]) was calculated. A DC value of 1 indicates perfect similarity between the volumes, while a value of 0 indicates no similarity.

In study III, necrotic tumor volume was manually outlined in preoperative MRI-T1-Gad, with guidance from standard T2-weighted and FLAIR images. Enhancing residual tumor volumes were correspondingly delineated in postoperative clinical MRI performed 1–4 days after operation.

4.5 Patient characteristics in the retrospective study (IV)

A retrospective analysis was performed on adult patients with newly diagnosed supratentorial glioma, grades II–IV, who underwent surgical resection or biopsy at Turku University Hospital from January 2005 through December 2013. A total of 184 glioma samples were obtained from Auria Biobank (TYKS-SAPA, Turku University Hospital, Turku, Finland). Clinical data were collected from the electronic patient data system. Tumor samples were studied for SSTR2A expression and established molecular markers. With all the molecular data available, gliomas were re-assessed by an experienced neuropathologist and diagnosed according to the new WHO classification (Louis et al. 2016).

4.6 Molecular markers in human gliomas (II, III, IV)

Formalin-fixed paraffin-embedded tumor tissues were sectioned at 3 μm (II, III) or 4 μm (IV) and used for analyses. Different antibodies employed for IHC are listed in Table 1. In studies II and III, all stainings were performed on whole tissue sections. In study IV, IHC for IDH1 R132H (the most common *IDH1* mutation), ATRX, and p53 mutation were performed using tissue microarray (TMA) blocks. TMA blocks were built by annotating most representative tumor areas in scanned H&E slides (Pannoramic Viewer, 3DHistech, Budapest, Hungary) and automatically transferring corresponding tissue cores from paraffin-embedded glioma samples into blocks using TMA Grand Master (3DHistech, Budapest, Hungary).

In studies II and III, *MGMT* promoter methylation was studied by pyrosequencing (Tuononen et al. 2012) and *EGFR* amplification by silver in situ hybridization (Ålgars et al. 2011). A 1p/19q codeletion was detected by fluorescent in situ hybridization using a Vysis 1p36/1q25 and 19q13/19p13 FISH probe kit (Abbot Laboratories, Abbot Park, IL). A p53 mutation was regarded as positive if nuclear staining was detected in more than 10% of neoplastic cells. EGFR IHC was reported using a scoring system previously described and also utilized for SSTR2A IHC (Ålgars et al. 2011). *ATRX* mutation was identified in case of lost nuclear staining in tumor cells while remaining positive in non-neoplastic cells.

In study IV, samples with negative or failed IDH1 IHC were subjected to direct Sanger sequencing to examine codons 132 and 172 in order to determine the mutation status of *IDH1* and *IDH2* genes, respectively. DNA was extracted from cylindrical paraffin-embedded tissue samples, and PCR amplification products were disposed to sequencing described by Hartmann et al. (Hartmann et al. 2009). Sequencing was performed in a forward direction at Eurofins Genomics (Ebersberg, Germany) using an ABI3730XL sequencer (ThermoFischer Scientific, MA, USA). The sequences were analyzed using Sequencer™ 5.1, and single ambiguous sequences after repetition were grouped in the NOS category.

4.7 SSTR2A immunohistochemistry in human gliomas (II, IV)

To disregard the expected SSTR2A expression in microglia and macrophages, SSTR2A IHC was performed as double staining using UMB-1 and CD68 antibodies. Double stainings were performed on whole paraffin tissue sections and not TMAs in order to also recognize the heterogeneous staining pattern.

Table 1 Primary antibodies and methods used for immunohistochemistry.

Antibody	Clone	Manufacturer	Method	Detection	Study
SSTR2	UMB-1	Abcam, Cambridge, UK	Ventana Benchmark XT Autostainer (Ventana Medical Systems, Strasbourg, France)	*ultra*VIEW Universal Detection Kit (Ventana, Strasbourg, France)	II, IV
SSTR3	Rabbit polyclonal (ab28680)	Abcam, Cambridge, UK	Labvision Autostainer (Thermo Scientific Inc., Kalamazoo, MI)	BrightVision Detection Kit (Immunologic, Duiven, the Netherlands)	II
SSTR5	Rabbit polyclonal (ab5681)	Millipore, Billerica, MA	Labvision Autostainer	BrightVision Detection Kit	II
EGFR	5B7	Ventana, Strasbourg, France	Ventana Benchmark XT Autostainer	*ultra*VIEW Universal Detection Kit	II, III
IDH1 R132H	H09	Dianova, Hamburg, Germany	Ventana Benchmark XT Autostainer	*ultra*VIEW Universal Detection Kit	II, III, IV
CD68	PG-M1	Dako, Glostrup, Denmark	Ventana Benchmark XT Autostainer[a]	*ultra*VIEW Universal Detection Kit + Universal Alkaline Phosphatase Red Detection Kit (Ventana)[a]	II, IV
Ki67	30-9	Ventana, Strasbourg, France	Ventana Benchmark XT Autostainer	*ultra*VIEW Universal Detection Kit	II, III
GFAP	EP671Y	Ventana, Strasbourg, France	Ventana Benchmark XT Autostainer	*ultra*VIEW Universal Detection Kit	III
p53	Bp53-11	Ventana, Tucson, AZ	Ventana Benchmark XT Autostainer	*ultra*VIEW Universal Detection Kit	II, IV
ATRX	Rabbit polyclonal (HPA001906)	Sigma-Aldrich, St Louis, MO	Ventana Benchmark XT Autostainer	*ultra*VIEW Universal Detection Kit	IV

[a]SSTR2 + CD68 double staining

The chromogen used for CD68 detection was red, while SSTR2A staining was brown.

Staining intensity for SSTR2A reaction was reported as 0 (negative), 1 (weak), 2 (moderate), or 3 (strong). Due to the heterogeneous staining pattern, we evaluated both the most common staining intensity (minimum 50% of tumor area) and the highest staining intensity (minimum 10% of tumor area). Additionally, the localization of staining (cytoplasmic, membranous, or both) was observed. SSTR2 IHC was scored first independently by an experienced neuropathologist and then in consensus with a research fellow. In study II, SSTR2A IHC was regarded as positive if the sum of the highest and most common staining intensities was ≥ 4. In study IV, SSTR2A IHC was regarded as positive if the most common staining intensity was 2 or 3, or if the highest staining intensity was 3. In study II, SSTR3 and SSTR5 IHC were also performed.

4.8 Serum GFAP and EGFR measurements (III)

Venous blood samples were centrifuged at 2500×*g* for 10 min and supernatants were stored at -70° C. Serum GFAP and EGFR levels were determined using commercially available sandwich enzyme-linked immunosorbent assay (ELISA) kits from BioVendor (Brno, Czech Republic) and OncogeneScience (Cambridge, USA), respectively. Samples were diluted 1:3 for GFAP ELISA and 1:50 for EGFR ELISA and were run in duplicates with a volume of 100 µl pipetted into each ELISA well. A biotin-labeled anti-GFAP-antibody and an alkaline phosphatase-labeled anti-EGFR-antibody specifically recognizing the extracellular domain of EGFR were employed. The absorbance was measured by reading the plate at 450 nm for GFAP and at 650 nm for EGFR. Reported concentration values are the mean absorbances of the duplicates. The limit of detection defined as the mean absorbance of the blanks (calibrator diluent) plus 3 SD ($A_{blank} + 3 \times SD_{blank}$) was measured and calculated as 0.014 ng/ml for GFAP. All values below this detection limit were defined as 0 ng/ml, which also was applied in case the other absorbance measurement of a duplicate was below the detection limit. Serum EGFR ELISA assays for HGG patients and control subjects were performed at separate times; therefore, 24 samples from HGG patients were re-analyzed for serum EGFR to test the reliability of the measurement.

4.9 Ethical considerations (I–IV)

All animal care and experiments were approved by the national Animal Experiment Board in Finland (21.12.2011 PH1296A) and carried out in compliance with Finnish laws relating to the conduct of animal experimentation. (I)

The registered prospective clinical study (ClinicalTrials.gov NCT01460706) was approved by the Ethics Committee of the Hospital District of Southwest Finland and the Finnish Medicines Agency. All patients and healthy control subjects gave written informed consent prior to participation. (II, III)

The retrospective study was approved by the Ethics Committee of the Hospital District of Southwest Finland and Auria Biobank. The samples were obtained from Auria Biobank (TYKS-SAPA, Turku University Hospital, Turku, Finland), and in accordance with the Finnish Biobank Act, a separate informed consent from individual patients was waived. (IV)

4.10 Statistical analysis

Data are presented as mean ± standard deviation. Normality was tested with the Shapiro-Wilk test. Comparisons between two variables were performed with a Student's t-test or the Mann-Whitney U test, with Bonferroni correction as appropriate for continuous and cross-tabulation with a Chi-square test or Fisher's exact test as appropriate for categorical variables. Comparisons between more than two variables were carried out with one-way ANOVA or a Kruskal-Wallis test as appropriate. Correlations between two variables were studied using Pearson or Spearman's rank correlation where applicable. A Kaplan-Meier with Log-Rank test and univariate and/or multivariate Cox proportional hazards regressions were performed to assess survival data. Overall survival (OS) was defined as the time from surgical resection to death or until the end of the follow-up. Progression-free survival (PFS) was defined as the time from surgical resection to tumor progression in MRI, deterioration in clinical symptoms, or the end of the follow-up (II, III), or as the time from surgical resection to the first tumor progression indicated by re-resection, the start of a new treatment regimen, death, or the end of the follow-up (IV). In study III, receiver operating characteristic (ROC) curve analysis was used to evaluate the ability of serum biomarkers to differentiate glioblastomas and to provide cutoff value for the Kaplan-Meier curve. Agreement between repeated measurements was assessed with intraclass correlation coefficient ICC (3,1) and Coefficient of Repeatability (CR).

All tests were two-sided, and statistical significance was set at $p < 0.05$. Statistical analyses were performed using SPSS Statistics software versions 17.0 for Mac (SPSS Inc., Chicago, IL,USA), 21.0 for Mac, or 24.0 (IBM Corp., Armonk, NY, USA).

5 RESULTS

5.1 BT4C glioma models (I)

Stereotactic BT4C injections induced orthotopic tumors in seven out of nine rats as confirmed by MRI 13 days after injection. All rats, however, underwent ^{68}Ga-DOTATOC PET/CT. H&E staining demonstrated orthotopic tumors with high cellularity and marked pleomorphism, small necrotic areas, neovascularization, and infiltrative border, mimicking human high-grade gliomas. Mean tumor size was 4 × 3 mm.

Subcutaneous BT4C xenografts were successfully induced into the neck and left limb of each mouse (n=16). Histologically, they resembled orthotopic BT4C gliomas, but without infiltrative border and with less neovascularization and necrosis. Mean tumor size was 5 × 5 mm.

5.1.1 Visualization of BT4C gliomas with SSTR2 PET/CT is limited

Rat orthotopic gliomas were only modestly visualized with ^{68}Ga-DOTATOC PET/CT. Tumor mean SUVmax (30–60 min post-injection) was 0.6 ± 0.3, and the ratio between the tumor and a contralateral normal brain was 2.0 ± 0.6. One PET/CT of a rat bearing a tumor failed due to wrong table positioning. In subcutaneous mice xenografts, the visualization was even poorer, with only 6/16 tumors detectable with ^{68}Ga-DOTATOC (mean SUVmax 0.4 ± 0.1) and 3/16 tumors detectable with ^{18}F-FDR-NOC (mean SUVmax 0.5 ± 0.1) PET/CT. In contrast, ^{18}F-FDG PET/CT showed an increased uptake in all 16/16 subcutaneous mice xenografts with mean scaled SUVmax of 1.4 ± 0.7.

5.1.2 *Ex vivo* biodistribution and autoradiography demonstrate tracer uptake in BT4C tumor

Ex vivo tissue radioactivity measurements at 60 min after injection are presented in Table 2. Subcutaneous mice xenografts showed a high uptake of both ^{68}Ga-DOTATOC and ^{18}F-FDR-NOC compared to the reference tissue muscle (^{68}Ga-DOTATOC $p = 0.001$, Mann-Whitney U test; ^{18}F-FDR-NOC $p < 0.001$, Student's t-test). The ^{18}F-FDR-NOC showed a higher uptake in both tumor and reference tissue, resulting in lower tumor-to-muscle ratios compared to ^{68}Ga-DOTATOC ($p = 0.002$, Mann-Whitney U test). Orthotopic rat gliomas were not analyzed with a gamma counter in order to obtain intact brain tumor for autoradiography analysis.

Table 2. *Ex vivo* tissue radioactivity measurements at 60 min after injection with ^{68}Ga-DOTATOC and ^{18}F-FDR-NOC. (Original publication I. Reprinted by permission of Taylor & Francis Ltd, www.informaworld.com).

	Rat orthotopic BT4C glioma	Mice subcutaneous BT4C tumor		
	^{68}Ga-DOTATOC n=9	^{68}Ga-DOTATOC n=8	^{18}F-FDR-NOC n=8	*P*
Tumor	NA	0.31±0.11	0.38±0.04	*
Muscle	0.10±0.04	0.05±0.02	0.08±0.01	*
Brain	NA	0.02±0.02	0.03±0.00	*
Heart	0.24±0.06	0.10±0.04	0.27±0.04	**
Lung	0.70±0.14	0.34±0.09	0.81±0.07	**
Liver	0.47±0.40	0.12±0.03	4.54±0.34	**
Pancreas	NA	0.63±0.23	0.68±0.23	
Spleen	0.56±0.57	0.10±0.03	0.25±0.04	**
Small intestine	0.60±0.20	0.18±0.05	1.42±0.69	**
Kidney	9.21±4.87	2.73±1.16	2.68±0.29	
Skin	0.33±0.09	0.31±0.11	0.41±0.05	*
Blood	0.65±0.16	0.28±0.12	0.71±0.10	**
Plasma	1.12±0.25	0.25±0.10	0.66±0.11	**
Urine	113±55.3	41.0±15.8	26.5±12.3	
Tumor-to-muscle ratio	NA	6.46±0.77	4.79±0.64	*
Tumor-to-brain ratio	NA	22.3±9.08	15.1±1.91	*

Results are expressed as SUVs (mean±SD). NA=not analyzed. *$p < 0.05$; **$p \leq 0.001$ between ^{68}Ga-DOTATOC and ^{18}F-FDR-NOC in nude mice bearing subcutaneous BT4C tumors.

Ex vivo biodistribution of ^{68}Ga-DOTATOC showed high values in the kidneys and urine and low values in other non-target organs, confirming the renal excretion of ^{68}Ga-DOTATOC. In contrast, ^{18}F-FDR-NOC was eliminated via the kidneys, but also via a hepatobiliary pathway, as indicated by signifantly increased radioactivity in the liver and small intestine compared to ^{68}Ga-DOTATOC ($p = 0.001$ for both tissues, Mann-Whitney U test).

In vivo stability of ^{68}Ga-DOTATOC in rat and mice plasma at 60 min after injection was excellent, with the percentage of intact ^{68}Ga-DOTATOC at 99–100%. Also, ^{18}F-FDR-NOC showed high *in vivo* stability with corresponding percentages of 94–96%.

Autoradiography analysis (Figure 3) demonstrated significant ^{68}Ga-DOTATOC uptake in the orthotopic rat glioma (9.8 ± 1.8 PSL/mm^2) compared to a contralateral normal brain (0.2 ± 0.1 PSL/mm^2, $p = 0.002$, Mann-Whitney U

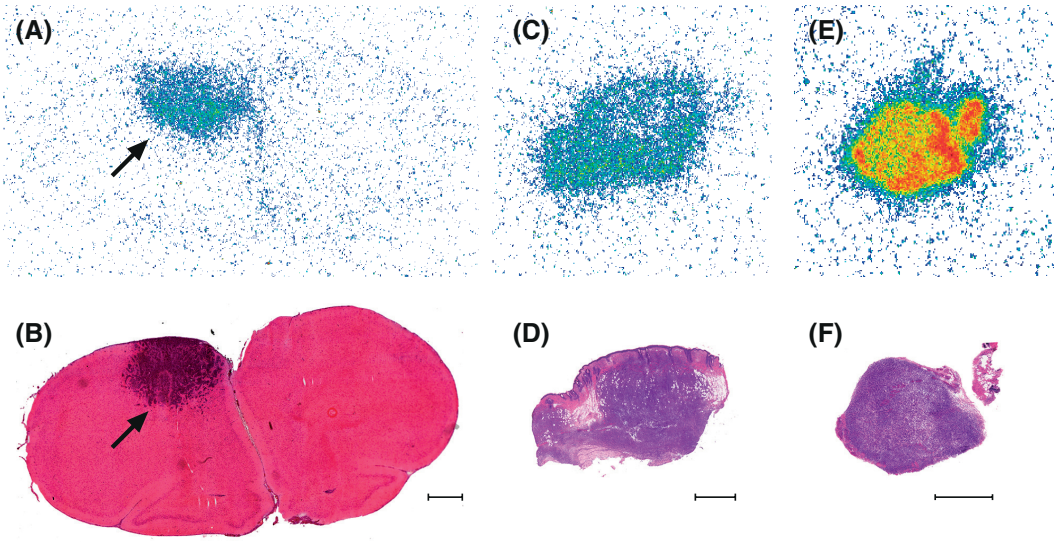

Figure 3. Autoradiography demonstrates high tumor uptakes of ^{68}Ga-DOTATOC and ^{18}F-FDR-NOC. Representative autoradiographs showing (A) an uptake of ^{68}Ga-DOTATOC in rat orthotopic BT4C glioma, (C) an uptake of ^{68}Ga-DOTATOC in subcutaneous BT4C tumor, and (E) an uptake of ^{18}F-FDR-NOC in another subcutaneous BT4C tumor. The (B, D, F) Lower panel shows H&E stainings of the corresponding sections. The Arrow indicates tumor in the rat brain. Bar = 1 mm (Original publication I. Reprinted with permission of Taylor & Francis Ltd, www.informaworld.com).

test) or muscle (1.2 ± 0.4 PSL/mm^2, p = 0.002) with a mean tumor-to-brain ratio of 68 ± 30 and tumor-to-muscle ratio of 9.2 ± 3.8. Also, subcutaneous mice xenografts presented high uptakes of both ^{68}Ga-DOTATOC (17 ± 7.5 PSL/mm^2) and ^{18}F-FDR-NOC (75 ± 18 PSL/mm^2) with mean tumor-to-muscle ratios of 6.7 ± 1.5 and 4.3 ± 0.8, respectively.

5.1.3 SSTR2 immunohistochemistry and Western blot analysis

Orthotopic rat gliomas showed positive SSTR2 staining in more than 95% of the tumor cells. The staining pattern was mainly cytoplasmic, but membranous staining was also detected. Subcutaneous mice xenografts showed more heterogeneous SSTR2 expression compared to orthotopic gliomas with positive staining in 40–80 % of the tumor cells.

Western blot analysis demonstrated SSTR2 expression of BT4C glioma cells by giving two major bands at ~30–32 kDa near the expected SSTR2 molecular size. Same major bands were detected in rat control tissue.

5.2 SSTR2 PET/CT in patients with high-grade gliomas (II)

5.2.1 ^{68}Ga-DOTA-peptide uptake associates with blood-brain barrier disruption

All 19 HGGs with tracer uptake demonstrated disrupted BBB in MRI, whereas no uptake was detected in tumors with intact BBB. Rapid peak in tumor uptake was followed by a gradual decline, reaching a plateau in 15 min. SUVmax in tumors with uptake was 2.3 ± 1.3 (range 0.5–5.7), and it correlated with $V_{T1\text{-}Gad}$ ($r = 0.713$, $p = 0.001$, Spearman's rank correlation). Binding potential (BP) was determined in patients with dynamic PET and tumor uptake. BP was 1.0 ± 1.1, and it correlated with tumor SUVmax ($r = 0.868$, $p < 0.001$). Negative BP values were found in HGGs with SUVmax < 1.0 and indicated a lower concentration of available receptors in the tumor compared to reference tissue (skin).

The difference in V_{PET} (9.3 ± 9.5 cm^3) and $V_{T1\text{-}Gad}$ (12.9 ± 11.7 cm^3) was nonsignificant ($p = 0.559$, Mann-Whitney U test). The $[V_{PET}]/[V_{T1\text{-}Gad}]$ tumor volume proportion was 1.05 ± 0.87. The dice similarity coefficient between V_{PET} and $V_{T1\text{-}Gad}$ was 0.41 ± 0.19.

5.2.2 ^{68}Ga-DOTA-peptide uptake does not correlate with SSTR2 expression by immunohistochemistry

SSTR2 IHC was positive in 9 HGGs and negative in 19 HGGs. Positive SSTR2 IHC was demonstrated in 4 out of 9 anaplastic astrocytomas, 2 out of 2 oligodendrogliomas, 2 out of 3 oligoastrocytomas, and 1 out of 2 glioblastomas with an oligodendroglioma component (GBMO). Negative SSTR2 IHC was shown in 10 glioblastomas, 1 secondary glioblastoma, and 1 gliosarcoma. SSTR2 IHC was not related to tracer uptake and SUVmax, as demonstrated in Figure 4. In fact, 7 out of 8 HGGs with no ^{68}Ga-DOTA-peptide uptake were classified as SSTR2 positive, while 17 out of 19 HGGs with tracer uptake were classified as SSTR2 negative. Since most HGGs demonstrated patchy areas of SSTR2 expression, though regarded as SSTR2 negative, we studied whether SUVmax or BP associates to the highest staining intensity observed. However, no association was found (SUVmax $p = 0.613$; BP $p = 0.655$, Kruskal-Wallis test).

SSTR3 immunoreactivity was detected in cells bordering necrosis in seven glioblastomas. One anaplastic astrocytoma displayed positive SSTR3 staining in approximately 30% of tumor cells. SSTR5 expression was not detected in any of the tumor specimens studied. SSTR2 expression in microglia and macrophages was not assessable due to intense CD68 reactivity. The

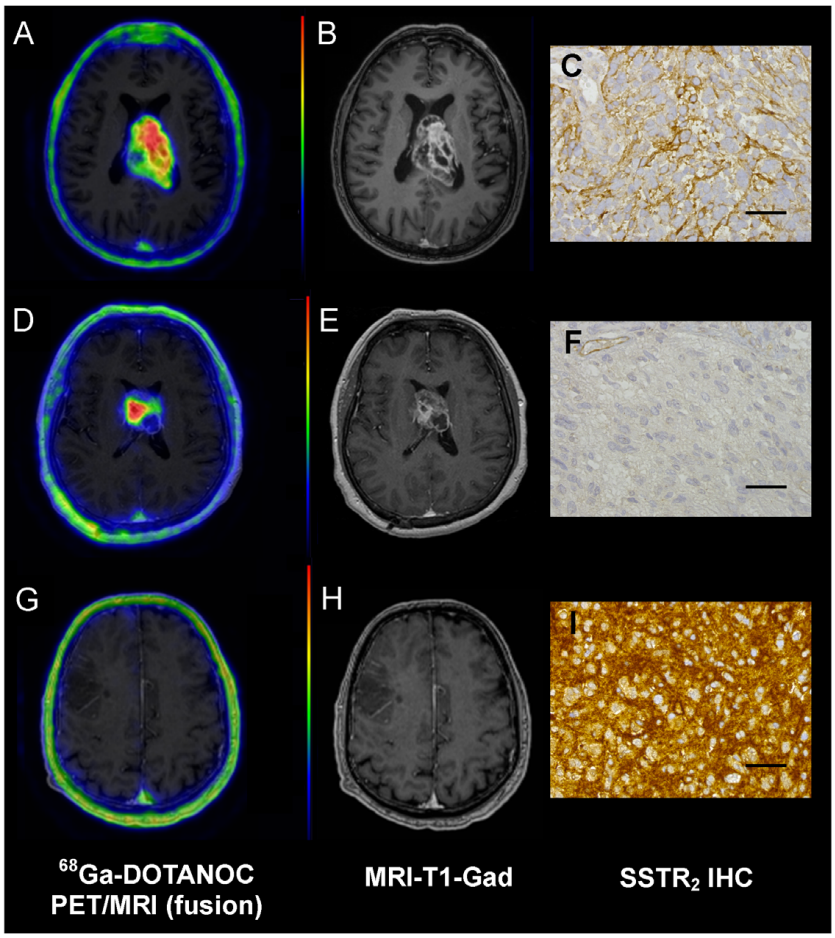

Figure 4. ^{68}Ga-DOTA-peptide uptake in high-grade gliomas does not correspond to SSTR2 immunohistochemistry. Axial-fused PET/MR images 30–60min post-injection, corresponding contrast-enhanced T1-weighted MR images, and tumor SSTR2 IHC from three different patients. Primary glioblastoma presents (A) ^{68}Ga-DOTANOC uptake, (B) contrast-enhancement in MRI-T1-Gad, and (C) patchy areas of positive SSTR2 staining. Another primary glioblastoma shows (D) ^{68}Ga-DOTANOC uptake and (E) contrast-enhancement. However, (F) SSTR2 IHC was negative. Primary oligoastrocytoma represents (G) no ^{68}Ga-DOTANOC uptake and (H) no contrast enhancement, but (I) high SSTR2 expression in IHC was detected. Color-scale in PET images is set to maximum (red) 10000 Bq/ml and minimum (blue) 0 Bq/ml. Bar = 50 µm (Original publication II. Reprinted with permission of SpringerOpen).

distribution and number of microglia and macrophages was heterogeneous. Within the cellular part of the tumor, variable diffuse infiltration was observed, whereas dense clusters of microglia and macrophages were detected along the necrosis border in glioblastomas.

5.2.3 Association of SSTR2 immunohistochemistry with molecular markers and survival

In our prospective PET/CT study including 28 HGG patients, positive SSTR2 IHC corresponded with *IDH1* mutation (p = 0.007, Chi-square test), lower

tumor grade (p = 0.005), and oligodendroglioma component (p = 0.010). Furthermore, Ki67 was significantly lower in SSTR2-positive HGGs (14.4 ± 10.5) compared to SSTR2-negative HGGs (41.1 ± 25.6, p = 0.001, Student's t-test). Association between SSTR2 IHC and *MGMT* promoter methylation was not significant (p = 0.080, Chi-square test), but it is notable that all SSTR2-positive HGGs contained *MGMT* promoter methylation, whereas all unmethylated HGGs were SSTR2 negative. Positive SSTR2 IHC was related to the absence of *EGFR* amplification (p = 0.021). However, no association was found between SSTR2 and EGFR IHC. In multivariate Cox regression analysis (backward Wald), SSTR2 expression was an independent prognostic factor for prolonged PFS after adjustment to histological grade (HR 0.161, CI 0.037–0.704, p = 0.015).

5.3 Serum GFAP and EGFR in high-grade glioma patients (III)

5.3.1 Preoperative serum GFAP

Of the patients, 12 out of 14 (86%) with glioblastoma and 3 out of 13 (23%) with anaplastic glioma had preoperatively detectable serum GFAP levels (≥ 0.014 ng/ml). All control subjects but one showed zero serum GFAP (detection limit 0.014 ng/ml). Serum GFAP was significantly higher in glioblastoma patients (0.079 ± 0.100) compared to anaplastic glioma patients (0.012 ± 0.028; p = 0.003, Mann-Whitney U test) or controls (p = 0.001). No difference was observed between anaplastic glioma patients and control subjects (p = 1.000). Serum GFAP levels for primary and recurrent HGGs were 0.055 ± 0.098 and 0.032 ± 0.038, respectively (p = 0.979).

Preoperative serum GFAP values significantly correlated to enhancing tumor volume and necrotic tumor volume in MRI both in primary (r = 0.64, p = 0.005 and r = 0.73, p = 0.001, respectively, Spearman's rank correlation) and in recurrent HGGs (r = 0.76, p = 0.011 and r = 0.64, p = 0.047, respectively).

Patients with *IDH1*-mutant HGGs showed significantly lower serum GFAP levels (0.012 ± 0.033 ng/ml) compared to *IDH1*-wildtype HGGs (0.061 ± 0.091 ng/ml, p = 0.016, Mann-Whitney U test). No difference in serum GFAP was observed in relation to 1p/19q codeletion or MGMT promoter methylation status. In contrast, serum GFAP values correlated to the Ki67 proliferation index (r = 0.78, p < 0.001, Spearman's rank correlation). All HGGs expressed GFAP detected by immunohistochemistry (GFAP-positive cells 87 ± 20%), the extent of which, however, did not correlate to serum GFAP levels (p = 0.761).

ROC analysis for the differentiation of glioblastoma from anaplastic glioma or control patients produced a serum GFAP cut-off value of 0.01 ng/ml with a sensitivity of 86% and a specificity of 85% (AUC 0.86, $p < 0.001$, CI 0.72–0.99). Univariate Cox regression analysis revealed that a serum GFAP value of > 0.01 ng/ml predicted poorer PFS in primary HGGs (Hazard ratio 5.9, $p = 0.032$, CI 1.2–29.9).

5.3.2 Preoperative serum EGFR

No statistical difference was observed in preoperative serum EGFR values between glioblastoma patients (52.6 ± 11.0 ng/ml), anaplastic glioma patients (50.6 ± 9.2 ng/ml), and control subjects (55.8 ± 7.8 ng/ml, $p = 0.391$, One-way ANOVA). Serum EGFR values did not correlate to enhancing or necrotic tumor volumes in MRI, nor to the Ki67 proliferation index. Furthermore, serum EGFR showed no variation in relation to IDH1, 1p19q, or *MGMT* status.

We tested the potential of serum EGFR as a surrogate marker for EGFR status in the tumor tissue. However, no association was found. No difference in serum EGFR was observed between HGG patients with EGFR amplification (54.5 ± 12.0 ng/ml) or without EGFR amplification (50.5 ± 9.2 ng/ml, $p = 0.351$, Student's t-test). All HGGs studied showed positive staining in EGFR immunohistochemistry, with the most common staining intensity varying from 0 to 3. Location was most commonly both cytoplasmic and membranous. Intensity or location of EGFR IHC, however, was not associated with serum EGFR ($p = 0.418$ and $p = 0.206$, respectively, Kruskal-Wallis test), nor with *EGFR* amplification ($p = 0.091$ and $p = 0.943$, respectively, Chi-square test). For repeated EGFR ELISA measurements, ICC(3,1) was 0.764 (CI 0.532–0.890) and CR 14.5 ng/ml, indicating a moderate agreement between measurements.

5.3.3 Postoperative serum GFAP and EGFR

A significant increase in postoperative serum GFAP levels was detected in 13 out of 20 (65%) HGG patients compared to preoperative values ($p = 0.003$, Wilcoxon signed-rank test). No correlation between postoperative serum GFAP and enhancing residual tumor volume in post-surgical MRI was found ($p = 0.372$, Spearman's rank correlation). Postoperative serum EGFR levels did not differ from those observed preoperatively ($p = 0.354$), nor did they correlate with enhancing residual tumor volume.

5.4 SSTR2A expression in the retrospective cohort of glioma samples (IV)

A total of 184 gliomas in the retrospective study included 101 glioblastomas (93 *IDH*-wildtype, 3 *IDH*-mutant, 5 NOS), 60 astrocytomas (22 *IDH*-wildtype, 37 *IDH*-mutant, 1 NOS), and 23 oligodendrogliomas (19 *IDH*-mutant and 1p/19q-codeleted, 4 NOS). Direct sequencing detected one *IDH2* mutation in a grade II astrocytoma, and six additional *IDH1* mutations were identified. Four oligodendrogliomas with 1p/19q codeletion and typical oligodendroglial histology were designated to the NOS group since *IDH1*/*IDH2* mutation could not be detected.

Representative IHC images of different staining intensities used for SSTR2A IHC scoring are shown in Figure 5. High SSTR2A expression significantly associated with oligodendrogliomas, whereas the majority of glioblastomas were negative for SSTR2A immunostaining (Table 3). SSTR2A expression

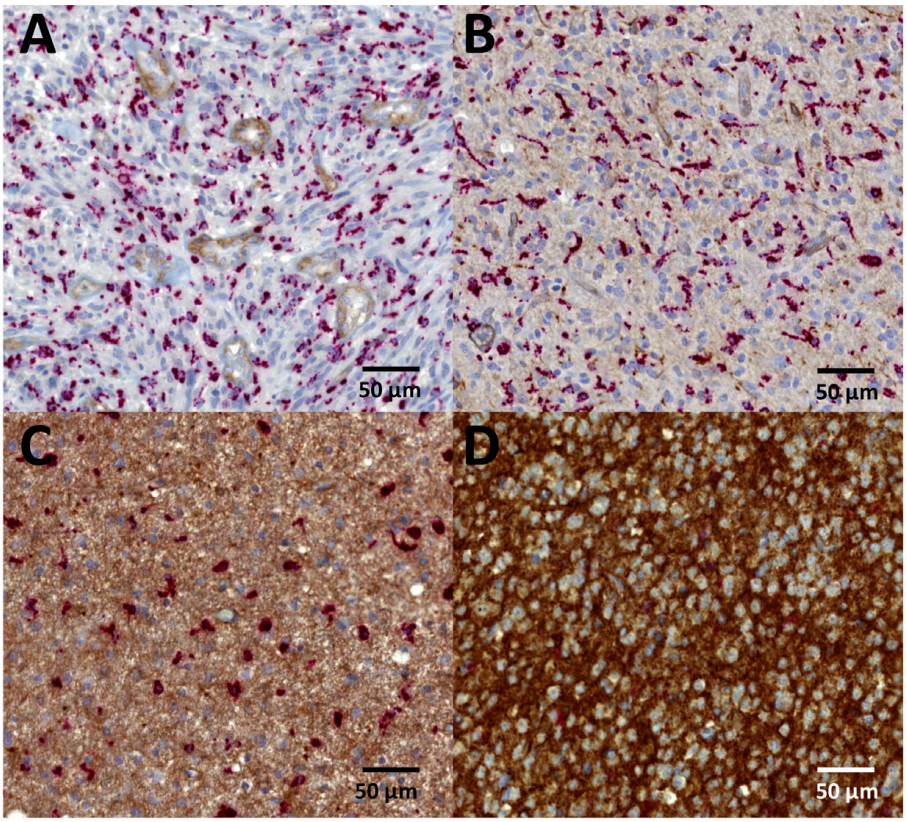

Figure 5. SSTR2A immunohistochemistry. Intensity of SSTR2A staining was scored as (A) 0=negative, (B) 1=weak, (C) moderate=2, or (D) strong=3. Location was designated to be (B, C) cytoplasmic or (D) both membranous + cytoplasmic. Endothelial cells served as an internal positive control. Diagnoses include glioblastoma (A, B), astrocytoma *IDH*-mutant (C), and oligodendroglioma *IDH*-mutant and 1p/19q-codeleted (D).

Table 3 SSTR2A IHC scoring in different glioma entities (IDHwt=IDH-wildtype, IDHmut=IDH-mutant, C=cytoplasmic, M+C=membranous+cytoplasmic)

		most common intensity				highest intensity				location	
		0	**1**	**2**	**3**	**0**	**1**	**2**	**3**	**C**	**M+C**
GLIOBLASTOMA (n)	IDHwt (n=93)	90	1	1	1	57	15	9	12	26	11
	IDHmut (n=3)	3	0	0	0	0	2	1	0	2	1
ASTROCYTOMA (n)	IDHwt (n=22)	19	2	1	0	12	2	3	5	10	0
	IDHmut (n=37)	24	5	5	3	9	9	10	9	24	4
OLIGODENDRO-GLIOMA (n)	IDHmut, 1p/19q-codel (n=19)	4	1	7	7	0	0	4	15	7	12

significantly varied between glioma entities evaluated by the most common staining intensity (minimum 50% of tumor area, $p < 0.001$, Fisher's exact test).

The most common pattern of SSTR2A staining was predominantly negative in glioblastomas (97%), *IDH*-wildtype astrocytomas (86%), and in the majority of *IDH*-mutant astrocytomas (65%). Within the negative tumor bulk, however, tumor cell clusters with intensive SSTR2A staining were identified, resulting in a heterogeneous staining pattern. We scored the tumor as SSTR2A positive if the most common intensity was 2 or 3, or if the highest intensity was 3. This translated to a positive SSTR2A IHC in 12 *IDH*-wildtype glioblastomas (13%), 5 *IDH*-wildtype astrocytomas (23%), 10 *IDH*-mutant astrocytomas (27%), and 15 *IDH*-mutant and 1p/19q-codeleted oligodendrogliomas (79%), demonstrating a significant association between SSTR2A expression and glioma type ($p < 0.001$, Fisher's exact test). Accordingly, SSTR2A expression was related to *IDH* mutation since the majority (60%) of SSTR2A-positive gliomas harbored *IDH* mutation ($p < 0.001$, Fisher's exact test). No association between SSTR2A expression and *ATRX* mutation was observed ($p = 0.469$).

In glioblastomas and astrocytomas, the SSTR2A expression was mainly located in the cytoplasm, whereas in the majority of oligodendrogliomas, the staining pattern was additionally membranous (Table 3, $p < 0.001$, Fisher's exact test). Oligodendrogliomas NOS (n=4) were not included in the final analyses, but it is noteworthy that they all presented an SSTR2A intensity of 3 as the most common staining. Furthermore, in three cases, the staining was mostly membranous, following the pattern of 1p/19q-codeleted tumors. A high number of CD68-positive microglia and macrophages were detected in the tumor zone, bordering necrosis in glioblastomas. No SSTR2A immunoreactivity in microglia and macrophages could be detected through the intense red staining of CD68.

No difference in OS or PFS was observed in glioblastomas according to SSTR2A status ($p = 0.173$ and $p = 0.114$, respectively, Log-Rank test). In contrast, patients with SSTR2A-positive grade II or III glioma showed clear survival benefit compared to SSTR2A-negative gliomas (OS $p = 0.005$, PFS $p = 0.052$, Log-Rank test). This benefit, however, may be related to the association between SSTR2A and oligodendrogliomas and their favorable outcome since no significant difference in OS ($p = 0.383$) or PFS ($p = 0.272$) was observed within *IDH*-mutant and *IDH*-wildtype astrocytomas. In the multivariate Cox regression analysis of grade II and III gliomas, both *IDH* mutation (HR 5.1, CI 2.4–11.0, $p < 0.001$) and positive SSTR2A (HR 2.7, CI 1.2–5.8, $p = 0.013$) remained independent factors that were significantly associated with longer overall survival after adjustment for age, preoperative KPS, and resection type.

6 DISCUSSION

6.1 BT4C glioma models express SSTR2

Experimental glioma models that study SSTR2-targeted therapies are warranted, as the clinical interest in SSTR2-targeted radionuclide therapy in gliomas has grown (Heute et al. 2010; Merlo et al. 1999; Schumacher et al. 2002). In addition, the detection of SSTR2 *in vivo* with PET/CT would be highly beneficial for the planning and follow-up of treatment strategies targeting SSTR2. Therefore, we examined SSTR2 status in two BT4C glioma models (orthotopic rat glioma and mice xenograft) and assessed whether SSTR2 expression could be visualized by PET/CT using two different tracers targeting SSTR2, ^{68}Ga-DOTATOC, and ^{18}F-FDR-NOC.

High tumor uptake of ^{68}Ga-DOTATOC was detected in orthotopic rat gliomas by autoradiography, indicating active receptor binding since DOTATOC predominantly binds to SSTR2 (Reubi et al. 2000). In line with this, SSTR2 expression was immunohistochemically observed in the majority of tumor cells. However, passive tumor accumulation of ^{68}Ga-DOTATOC in addition to active binding cannot be ruled out since orthotopic rat BT4C gliomas are known to manifest disrupted BBB, as indicated by MRI contrast enhancement (Thorsen et al. 2003). The cytoplasmic location of the SSTR2 immunostain corresponds to a previous *in vivo* study, in which internalization of membranous SSTR2 in rat AR42J tumor cells was already seen 2.5 min after intravenous injection of the SSTR2 agonist and was still detectable 6 h after injection (Waser et al. 2009). In our study, SSTR2 IHC was performed on tissue samples collected 60 min after intravenous injection with ^{68}Ga-DOTATOC. Unfortunately, in this study we did not analyze SSTR2 IHC from intervention-naïve rat gliomas.

Mice with BT4C xenografts underwent PET/CT with ^{68}Ga-DOTATOC, ^{18}F-FDR-NOC, and also ^{18}F-FDG. High tumor uptake of both ^{68}Ga-DOTATOC and ^{18}F-FDR-NOC were detected by autoradiography but also by *ex vivo* tissue radioactivity measurements. SSTR2 IHC was positive in xenografts, but showed more heterogeneous expression compared to orthotopic gliomas. Moreover, Western blot detected SSTR2 expression in the BT4C cell line. Despite the positive *ex vivo* results, however, ^{68}Ga-DOTATOC and ^{18}F-FDR-NOC performed rather poorly with PET imaging *in vivo*. Autoradiography is known to have higher sensitivity compared to PET, especially with small target lesions (Schmidt and Smith 2005). Since mean tumor size in orthotopic gliomas was only 4 × 3 mm, it can be speculated that ^{68}Ga-radionuclide may not be optimal for imaging small target lesions due

to its high positron energy and corresponding large positron range in tissue, resulting in limited spatial resolution and lower image quality.

We employed a novel tracer, ^{18}F-FDR-NOC, to study whether glycosylation of the tracer peptide would improve tumor uptake and induce sufficient signal intensity for visualization with PET (Li et al. 2014). Elevated tumor uptake and high tumor-to-organ ratios have previously been reported using SSTR2 agonists conjugated with different carbohydrates such as glucose and maltose (Schottelius et al. 2002). In mice xenografts, significantly higher tumor uptake was detected with ^{18}F-FDR-NOC compared to ^{68}Ga-DOTATOC by autoradiography and *ex vivo* radioactivity measurements. Tumor visualization with ^{18}F-FDR-NOC PET/CT, however, was not improved. Furthermore, we found a high uptake of ^{18}F-FDR-NOC in almost all non-target organs, including the liver corresponding to less-favorable pharmacokinetics and excretion via the hepatobiliary pathway compared to ^{68}Ga-DOTATOC, which is eliminated exclusively through the kidneys.

We conclude that orthotopic rat BT4C glioma and mice BT4C xenograft express SSTR2 as demonstrated with autoradiography, tissue radioactivity measurements, IHC, and Western blotting. Especially orthotopic rat BT4C glioma is warranted to be further evaluated in treatment strategies targeting SSTR2. Unfortunately, *in vivo* PET/CT with ^{68}Ga-DOTATOC or ^{18}F-FDR-NOC provides limited value in the follow-up due to low tumor signal.

6.2 SSTR2 PET/CT provides limited value in identifying patients with high-grade glioma suitable for radionuclide therapy

In our prospective clinical study with HGG patients, we demonstrated that ^{68}Ga-DOTA-peptide uptake in PET/CT is associated with disrupted BBB but does not correlate with an immunohistochemically determined SSTR2 status, suggesting limited benefit of this approach in defining suitable patients for radionuclide therapy. Our findings correspond to SSTR scintigraphic studies in low- and high-grade gliomas, in which ^{111}In-DTPA-D-Phe1-octreotide scintigraphy visualized the tumors with disrupted BBB but did not correlate to *in vitro* SSTR autoradiography (Haldemann et al. 1995). The authors concluded that this discrepancy was due to nonspecific accumulation. Although we detected variation in SUVmax among similar MRI tumor volumes and alterations in PET binding potential values suggesting different SSTR2 densities in HGGs, we conclude that receptor expression in HGGs with disrupted BBB is too low for specific receptor binding to be responsible for the tracer uptake.

High tumor uptake in SSTR2 PET/CT is associated with the efficiency of radionuclide therapy. In meningiomas treated with radionuclide therapy, SUVmax with ^{68}Ga-DOTA-peptides was related to the corresponding ^{177}Lu-labeled radionuclide uptake and therapeutic dose (Hanscheid et al. 2012). SUVmax in meningiomas ranged from 4.3 to 68.7, with a very low therapeutic dose achieved with the lowest SUVmax. In our study, mean SUVmax was 2.25 with only four GBMs and one anaplastic glioma, demonstrating an SUVmax > 3.0 and suggesting an insufficient achievable dose in radionuclide therapy. However, it must be noted that radionuclide therapy in extra-axial meningiomas is intravenously delivered, whereas in gliomas invading the brain, the therapeutic radionuclide needs to be locally injected (Heute et al. 2010; Merlo et al. 1999; Schumacher et al. 2002). This is important, especially in HGGs with intact BBB that are SSTR2 positive but lack tracer uptake in PET. These tumors may benefit from locally delivered radionuclide therapy, but they cannot be evaluated by intravenously given ^{68}Ga-DOTA-peptides.

Of particular interest was the finding of a positive association between SSTR2 expression and the oligodendroglioma component, *IDH1* mutation, and improved PFS. Previous studies have not detected a clear association between SSTR2 expression and oligodendrogliomas. Cervera et al. found increased SSTR2 mRNA in oligodendrogliomas, but finally concluded that it was due to contamination from a normal brain (Cervera et al. 2002). In contrast, our SSTR2 detection was based on IHC allowing cellular and sub-cellular localization. Cortical neurons and neuropile are known to express SSTR2, which was also detected in our samples. These areas, however, were not included since the scoring of SSTR2 IHC was performed on tumor cells and regions with the highest cellularity.

Our results suggest a prognostic value for SSTR2 in high-grade gliomas. First, SSTR2 remained as an independent marker for improved PFS after adjustment to the glioma grade. Second, SSTR2 expression associated with *IDH1* mutation, which is regarded as the most powerful prognostic factor predicting favorable outcome compared to *IDH1* wild-type gliomas (Horbinski 2013). These results substantiate the anti-oncogenic role of SSTR2 in HGGs. The number of patients, was limited, however, and we therefore concluded that the potential diagnostic and prognostic values of SSTR2 should be confirmed in a larger study.

6.3 High serum GFAP associates with tumor burden in both primary and recurrent high-grade gliomas

Established molecular diagnostics are made from biopsied or surgically resected tumor tissue. Intratumor heterogeneity, however, may cause sampling bias, and serial biopsies in the course of the follow-up are not practicable. We were interested in the potential of "liquid biopsy" to determine tumor burden and patient outcome. There is increasing evidence that serum GFAP is a potential biomarker for diagnosing glioblastomas from lower-grade gliomas and other space-occupying cerebral lesions (Jung et al. 2007; Tichy et al. 2016). Consistent with the literature, we found elevated serum GFAP in 86% of glioblastoma patients, but only 23% of patients with anaplastic glioma. With serum GFAP above 0.014 ng/ml, a sensitivity of 86% and a specificity of 85% for the diagnosis of glioblastoma was obtained.

Serum GFAP levels correlated with both enhancing and necrotic tumor volumes consistent with previous studies (Brommeland et al. 2007; Husain et al. 2012). This suggests that a critical amount of tumor tissue with BBB dysfunction is required for detectable serum levels, but also tumor necrosis with structural disintegration is involved in releasing circulating GFAP (Jung et al. 2007; Tichy et al. 2016).

The correlation of serum GFAP to enhancing tumor volume in recurrent HGGs is of interest, suggesting a possible value of serum GFAP as a biomarker for tumor recurrence. Previously this association has been evaluated only in primary HGGs [8, 10]. Tumor progression is routinely evaluated using contrast-enhanced MRI, however, which may be complicated by treatment-related changes such as pseudoprogression or pseudoresponse (Hygino da Cruz et al. 2011). Difficulties in determining true recurrence from these changes in MRI underlines the potential importance of our finding. A longitudinal follow-up with a larger patient population is warranted to study in more detail the ability of serum GFAP to detect recurrent HGGs at the earliest possible stage.

The relation of high-serum GFAP to *IDH*-wildtype HGGs and a high Ki67 proliferation index is most likely due to the strong association between elevated serum GFAP and glioblastomas. High-serum GFAP (0.014 ng/ml as a cutoff value) predicted poor PFS in HGG patients. Unfortunately, the number of subjects in this study was too low to examine the effect of serum GFAP on survival in glioblastomas only.

The increase in serum GFAP levels after surgical tumor resection is consistent with a previous study, which showed that plasma GFAP values were elevated

24–48 h after surgery in 83% of patients, including both low-grade and high-grade gliomas (Husain et al. 2012). No association was found between postoperative serum GFAP and enhancing residual tumor volume, indicating that postoperative circulating GFAP represents brain injury induced by the surgery itself rather than as a measure of residual tumor burden.

Elevated concentrations of circulating EGFR have been associated with various cancers, including cervical and gastric carcinomas, and pleural mesotheliomas (Choi et al. 1997; Gaafar et al. 2010; Oh et al. 2000). One study reports elevated serum EGFR in patients with glioblastomas (Quaranta et al. 2007). However, we were unable to detect any difference in serum EGFR levels among patients with glioblastoma, anaplastic glioma, and healthy controls. Furthermore, EGFR gene amplification or protein overexpression in tumor tissue were not related to circulating EGFR levels. These results suggest that BBB disruption does not affect the release of extracellular domain of EGFR into circulation and that tumor cells are not likely to be the major source of circulating EGFR in patients with HGG. This is supported by the fact that serum EGFR levels did not correlate to tumor burden in MRI. Our results indicate that serum EGFR has no diagnostic or prognostic value in patients with HGG, and it is not applicable as a predictive marker for efficacy or treatments targeting EGFR.

In our study, all HGGs demonstrated positive EGFR IHC with varying degrees of intensity and location. It is noteworthy, however, that this method is not strictly quantitative and the outcome not necessarily proportional to other studies due to the lack of standardized criteria for evaluation (scoring system) and methods used (e.g., storage time of the tumor tissue and the choice of primary antibody) (Barker et al. 2001; Burel-Vandenbos et al. 2013; Martin, Mazzucchelli, and Frattini 2009). Our EGFR IHC scoring was based on whole tissue sections, including the focal staining of both membranous and cytoplasmic location, resulting in high sensitivity, yet observing the divergence within the cohort.

6.4 High SSTR2A expression associates with oligodendrogliomas and improved survival

Studies on SSTR2 expression in gliomas have demonstrated remarkably controversial results (Dutour et al. 1998; Mawrin et al. 2004; Reubi et al. 1987). Our retrospective analysis included a total of 184 gliomas and is the most extensive effort to characterize SSTR2 expression in different glioma subtypes assessed by the 2016 WHO classification system. In our cohort, SSTR2A expression was significantly associated with oligodendrogliomas

(79% SSTR2A positive) compared to *IDH*-mutant or *IDH*-wildtype astrocytomas (27% and 23%, respectively) and especially glioblastomas, of which only 13% were SSTR2A positive.

Previous contradictory results on SSTR2 expression in glioma entities may be explained by the limitations in size and the analytical methods of these studies (Dutour et al. 1998; Mawrin et al. 2004; Reubi et al. 1987). First, the number of tumor samples, especially oligodendrogliomas, has been low. Furthermore, autoradiography or Northern blot analyses are unable to define the exact location of SSTR2 expression, and IHC with polyclonal antibodies may display cross-reactivity with other antigens (Reubi et al. 1999). Since human macrophages are known to express SSTR2 (Armani et al. 2007), we excluded their interference in the analyses by using double staining with CD68-targeting macrophages and UMB-1. UMB-1 is a monoclonal antibody providing robust staining compared to polyclonal antisera and is generally recommended as the method of choice for SSTR2A IHC (Fischer et al. 2008; Korner et al. 2012).

High SSTR2A expression in oligodendrogliomas carries clinical implications. First, intensive membranous and cytoplasmic SSTR2A staining detected in the majority of tumor cells may add diagnostic value to routine pathologic evaluation since membranous staining was almost exclusively limited to oligodendrogliomas. Four oligodendrogliomas in our cohort with 1p/19q codeletion and typical oligodendroglial histology were designated to the NOS group since no *IDH1*/*IDH2* mutation could be detected. Interestingly, all four tumors showed intensive SSTR2A expression. We hypothesize that intense membranous and cytoplasmic SSTR2A expression could act as a surrogate marker, supporting the diagnosis of oligodendroglioma in case of ambiguous or unavailable analysis of 1p19q or IDH status.

The second clinical implication of SSTR2A expression in gliomas is the therapeutic target it may offer. We demonstrated in our prospective study that PET/CT imaging with intravenously injected ^{68}Ga-DOTA-peptide targeting SSTR2 provides limited value in defining suitable patients with high-grade glioma for targeted radionuclide therapy. Thus, not only receptor expression and density but also the route of administration seems to be essential for targeted treatment in the case of gliomas.

Our results further question the role of SSTR2-targeted radionuclide therapy in glioblastomas. We characterized SSTR2A expression in 101 glioblastomas and demonstrate completely negative SSTR2 IHC in the majority of tumor samples. In contrast, we found that most oligodendrogliomas showed intense SSTR2A expression. Moreover, SSTR2A expression in oligodendrogliomas

was mostly localized to the plasma membrane of tumor cells in addition to concurrent cytoplasmic staining. Membranous SSTR2A is known to rapidly internalize after the binding of somatostatin analog, and this accumulation of internalized radioligand into tumor cells is considered the basis for successful radionuclide therapy (Waser et al. 2009). Consequently, the pattern of expression favors the theranostic approach using ^{90}Y-DOTATOC and ^{177}Lu-DOTATATE, and it might contribute to the treatment armamentarium of oligodendrogliomas, which should be addressed in future clinical trials.

SSTR2 itself is considered to be a tumor suppressor, and its expression has been associated with favorable outcomes in patients with pancreatic NETs and childhood neuroblastomas (Okuwaki et al. 2013; Raggi et al. 2000). Our study clearly supports similar survival benefits in patients with grade II–III glioma who present with positive SSTR2A IHC. This may be related to the strong association between SSTR2A expression and oligodendrogliomas, which typically demonstrate longer survival times than diffuse astrocytomas. However, the prognostic significance of SSTR2A cannot be trivialized since it remained an independent prognostic factor in the multivariate analysis, where *IDH* mutation and clinical determinants were included. Unfortunately, the number of patients in our study was too low to perform a separate survival analysis including oligodendrogliomas only. A recent study identified three subgroups of 1p/19q-codeleted oligodendroglial tumors having divergent outcomes by an integrated analysis of transcriptome, genome, and methylome (Kamoun et al. 2016). This study emphasizes the heterogeneity among oligodendrogliomas, and the role of SSTR2A expression in the three subgroups remains to be elucidated.

To our knowledge, this retrospective study is the most extensive one aiming to characterize SSTR2A expression in adult gliomas. Here we confirm our preliminary observation, implicating the association of SSTR2A expression with beneficial outcomes and oligodendroglial differentation where it may provide diagnostic and therapeutic value complementing the new molecular classification. In contrast, glioblastomas present negative or small patchy areas of SSTR2A staining, supporting the observation that glioblastomas are composed of numerous different clones with variable biological properties, where a theranostic approach using DOTA-labeled peptides is given low priority.

6.5 Limitations

Our prospective clinical study has several limitations. First, the number of patients was limited. However, the association between tracer uptake in PET/

CT and BBB disruption was apparent in only 27 patients. Furthermore, a larger retrospective study was conducted to validate the potential diagnostic and prognostic values of SSTR2 suggested by this pilot study. Secondly, we used two PET tracers with different affinity profiles for SSTR subtypes. However, the highest affinity with both ^{68}Ga-DOTANOC and ^{68}Ga-DOTATOC is for SSTR2 (Reubi et al. 2000). In addition, our HGG samples demonstrated minimal expression of SSTR3 and SSTR5, for which ^{68}Ga-DOTANOC possesses a higher affinity compared to ^{68}Ga-DOTATOC. Also, since ^{68}Ga-DOTATOC was applied in only 3 patients and ^{68}Ga-DOTANOC in 24, we conclude that this limitation most likely had little effect on the outcome. Third, potential alteration in tumor edema affecting volumetric analyses between MRI and PET/CT cannot be excluded. Fourth, ELISA tests for GFAP and EGFR are not standardized, and are thus for research use only. Furthermore, confirmation in larger cohorts is required for our preliminary results on serum GFAP as a potential indicator of tumor recurrence. The major limitation in our retrospective cohort was the limited number of oligodendrogliomas included. Future studies are warranted to evaluate the prognostic value of SSTR2 expression within oligodendrogliomas only.

7 CONCLUSIONS

Study I: Orthotopic rat BT4C glioma and mice BT4C xenograft express SSTR2 as demonstrated with autoradiography, tissue radioactivity measurements, IHC, and Western blotting, suggesting that these experimental glioma models may be of value in the treatment strategies targeting SSTR2. PET/CT with ^{68}Ga-DOTATOC or ^{18}F-FDR-NOC, however, provide limited value in the follow-up.

Study II: PET/CT with ^{68}Ga-DOTA-peptides provides limited value in identifying patients with SSTR2-positive HGGs suitable for radionuclide therapy. SSTR2 expression, however, was found to be associated with an oligodendroglioma component, *IDH1* mutation, and improved PFS, with potential diagnostic and prognostic values.

Study III: High serum GFAP associates with glioblastoma and poor PFS. Correlation with tumor burden in recurrent HGGs implicates the potential of serum GFAP as an indicator of tumor recurrence and should be addressed in future clinical trials. In contrast, circulating EGFR is not related to tumor EGFR expression and thus provides no value in EGFR-targeted therapies.

Study IV: Oligodendrogliomas present with high membranous and cytoplasmic SSTR2A expression with potential diagnostic and therapeutic value. Preliminary results in study II were further confirmed since SSTR2A expression associated with longer survival in grade II–III gliomas. In contrast, SSTR2A expression is infrequent in astrocytomas and negative in the majority of glioblastomas, questioning the role of SSTR2-targeted radionuclide therapy in glioblastomas.

ACKNOWLEDGMENTS

This study was conducted at the Turku PET Centre and the Department of Clinical Physiology and Nuclear Medicine in Turku University Hospital and the University of Turku during the years 2010–2017. I express my sincere appreciation to Professor Jaakko Hartiala (head of the Department of Clinical Physiology and Nuclear Medicine at the time of the study), Docent Jukka Kemppainen (head of the Department of Clinical Physiology and Nuclear Medicine since May 2016), and Professor Juhani Knuuti (Director of the Turku PET Centre) for providing the excellent facilities for my research.

I wish to express my deepest gratitude to my supervisors, Professor Heikki Minn and Professor Anne Roivainen. Heikki's exceptional talent as an awarded and enthusiastic scientist, recognized clinician, and head of department, while remaining sympathetic and down-to-earth never stops impressing me. Heikki's broad knowledge on gliomas in both clinical and research contexts has been invaluable and highly motivating in reaching this goal. I warmly thank Anne, especially for the guidance in the beginning of my project and preclinical studies, during which her deep comprehension on PET tracers and imaging were invaluable.

There are no words to describe how grateful I am to neuropathologist Maria Gardberg for her enormous input for this study. Her insightfulness in neuropathology, practical approach, and sincere attitude in teaching and helping me to understand the challenging world of neuropathology have been the basis of this work, and without her dedication, this study would have never been finished.

I wish to thank all my coauthors for their valuable contributions to this study. I warmly thank Professor Riitta Parkkola for the guidance in brain tumor MRI, and for the encouraging spirit she brings. Neurosurgeons Janek Frantzén and Ville Vuorinen are deeply appreciated for recruiting patients. I warmly thank Marko Pesola for helping in image analysis, and Jukka Kemppainen for the guidance in brain tumor PET. I express my gratitude to Anu Autio for teaching me analyses in preclinical studies, and to Heidi Liljenbäck for her excellent performance of animal studies. I wish to thank Xiang-Guo Li, Meeri Käkelä, Henri Sipilä, and Pauliina Luoto for establishing and manufacturing PET tracers. I warmly thank Tuula Tolvanen for setting up PET imaging parameters, Sami Suilamo for post-processing, and Jarkko Johansson for quantitative PET analyses. Seppo Ylä-Herttuala and Jere Kurkipuro are acknowledged for their guidance in setting up the animal studies, and Vanina D. Heuser for performing Western blot analyses. I thank Katri Kivinen for rapid DNA sequencing analyses. Jussi Posti, Jussi Sipilä, Melissa Rahi, and

Matti Sankinen are acknowledged for their contributions in collecting clinical data.

I am sincerely grateful to Professor Ritva Vanninen and Docent Hannu Haapasalo for their constructive and valuable comments during the revision process of this thesis. I warmly thank the members of my follow-up committee Professor Riitta Parkkola and Docent Sirkku Jyrkkiö.

I wish to thank the expert staff at Turku PET Centre. The radiographers Minna Aatsinki, Tarja Keskitalo, Hannele Lehtinen, and Marjo Tähti, and the medical laboratory technologists Sanna Suominen and Eija Salo, and all the IT-experts are sincerely appreciated for their skilled work in this project. I warmly thank all my fellow-researchers in Turku PET Centre for the helpful and easy-going atmosphere. Research coordinator Kirsi Penttilä is acknowledged for her practical help.

It is a privilege to be surrounded by suberb colleagues and coworkers in the Department of Radiology in Turku University Hospital. Professor Hannu Aronen is sincerely appreciated for the enthusiastic attitude toward science and research. I wish to express my gratitude to Docent Roberto Blanco-Sequeiros for his dynamic leadership. I warmly thank Johanna Virtanen for her support in the field of research. I wish to thank Pirkko, Tiina, Minna, Satu, Ia, Milja, Carita, Laura, Juho, Gaber, Mikko, Teemu, Ville T, Ville J, and each one of my fantastic colleagues for their friendliness and help, and for keeping up the spirit.

I am privileged to have many dear friends who make life a bit more easy and lighter every time we meet. I warmly thank Pauliina, my soul mate, for all the conversations and support. I wish to thank Eeva, Saara, Jonna, Maijastiina, Inari, Mari, Annukka, Satu-Maria and Laura for their friendship starting from day one in medical school. I thank Eeva Heiro for a friendship of decades. Hanna and Heikki, Anssi and Helena, Mikko and Sanna, Pia and Janne, Liisa and Tuukka, thank you for all the merry gatherings with this merry group.

I express my deepest gratitude to my parents, Paula and Ari Steiner, who have always supported me in my ambitions. I will always be obliged to my mother for the practical help she has unselfishly given us in everyday life during these busy years. I warmly thank my wonderful sisters Lara and Nora for a friendship that only sisters know exists. I thank Lara's and Nora's husbands, Tuomas and Tuomas, my brother Rudi and his wife Jenni, and their children for the numerous joyful and chaotic gatherings we have had with 13 small children. I wish to thank my mother-in-law Kaija and father-in-law Oskari for all the help and support they have given us. Above all, I thank my beloved

husband Tuomas for his love, support, and patience in sharing his life with me. Your enthusiastic and unyielding attitude for science has always inspired me and pushed me to reach this goal. You, Kauri, Vellamo, and Ellinoora mean the world to me.

The study was financially supported by the Cancer Society of Finland, Instrumentarium Science Foundation, the Hospital District of Southwest Finland and the Medical Imaging Centre of Southwest Finland (EVO-funding), Orion Research Foundation, Finnish Society of Oncology, Cancer Society of Southwest Finland, Finnish Society of Neuroradiology, Radiological Society of Finland, and the National Graduate School of Clinical Investigation.

Turku, March 2017

Aida Kiviniemi

REFERENCES

Adori C, Gluck L, Barde S, Yoshitake T, Kovacs GG, Mulder J, Magloczky Z, Havas L, Bolcskei K, Mitsios N, et al. 2015. Critical role of somatostatin receptor 2 in the vulnerability of the central noradrenergic system: New aspects on Alzheimer's disease. Acta Neuropathol 129(4):541-63.

Armani C, Catalani E, Balbarini A, Bagnoli P, Cervia D. 2007. Expression, pharmacology, and functional role of somatostatin receptor subtypes 1 and 2 in human macrophages. J Leukoc Biol 81(3):845-55.

Barbieri F, Pattarozzi A, Gatti M, Porcile C, Bajetto A, Ferrari A, Culler MD, Florio T. 2008. Somatostatin receptors 1, 2, and 5 cooperate in the somatostatin inhibition of C6 glioma cell proliferation in vitro via a phosphotyrosine phosphatase-eta-dependent inhibition of extracellularly regulated kinase-1/2. Endocrinology 149(9):4736-46.

Barbieri F, Pattarozzi A, Gatti M, Aiello C, Quintero A, Lunardi G, Bajetto A, Ferrari A, Culler MD, Florio T. 2009. Differential efficacy of SSTR1, -2, and -5 agonists in the inhibition of C6 glioma growth in nude mice. Am J Physiol Endocrinol Metab 297(5):E1078-88.

Barker FG 2nd, Simmons ML, Chang SM, Prados MD, Larson DA, Sneed PK, Wara WM, Berger MS, Chen P, Israel MA, et al. 2001. EGFR overexpression and radiation response in glioblastoma multiforme. Int J Radiat Oncol Biol Phys 51(2):410-18.

Barth RF and Kaur B. 2009. Rat brain tumor models in experimental neuro-oncology: The C6, 9L, T9, RG2, F98, BT4C, RT-2 and CNS-1 gliomas. J Neurooncol 94(3):299-312.

Bartolomei M, Bodei L, De Cicco C, Grana CM, Cremonesi M, Botteri E, Baio SM, Arico D, Sansovini M, Paganelli G. 2009. Peptide receptor radionuclide therapy with (90)Y-DOTATOC in recurrent meningioma. Eur J Nucl Med Mol Imaging 36(9):1407-16.

Basu S, Kwee TC, Surti S, Akin EA, Yoo D, Alavi A. 2011. Fundamentals of PET and PET/CT imaging. Ann N Y Acad Sci 1228:1-18.

Belosi F, Cicoria G, Lodi F, Malizia C, Fanti S, Boschi S, Marengo M. 2013. Generator breakthrough and radionuclidic purification in automated synthesis of ^{68}Ga-DOTANOC. Curr Radiopharm 6(2):72-77.

Best MG, Sol N, Zijl S, Reijneveld JC, Wesseling P, Wurdinger T. 2015. Liquid biopsies in patients with diffuse glioma. Acta Neuropathol 129(6):849-65.

Bodei L, Mueller-Brand J, Baum RP, Pavel ME, Horsch D, O'Dorisio MS, O'Dorisio TM, Howe JR, Cremonesi M, Kwekkeboom DJ, et al. 2013. The joint IAEA, EANM, and SNMMI practical guidance on peptide receptor radionuclide therapy (PRRNT) in neuroendocrine tumours. Eur J Nucl Med Mol Imaging 40(5):800-16.

Boy C, Heusner TA, Poeppel TD, Redmann-Bischofs A, Unger N, Jentzen W, Brandau W, Mann K, Antoch G, Bockisch A, et al. 2011. ^{68}Ga-DOTATOC PET/CT and somatostatin receptor (sst1-sst5) expression in normal human tissue: Correlation of sst2 mRNA and SUVmax. Eur J Nucl Med Mol Imaging 38(7):1224-36.

Brommeland T, Rosengren L, Fridlund S, Hennig R, Isaksen V. 2007. Serum levels of glial fibrillary acidic protein correlate to tumour volume of high-grade gliomas. Acta Neurol Scand 116(6):380-84.

Burel-Vandenbos F, Turchi L, Benchetrit M, Fontas E, Pedeutour Z, Rigau V, Almairac F, Ambrosetti D, Michiels JF, Virolle T. 2013. Cells with intense EGFR staining and a high nuclear to cytoplasmic ratio are specific for infiltrative glioma: A useful marker in neuropathological practice. Neuro Oncol 15(10):1278-88.

Cairncross G, Wang M, Shaw E, Jenkins R, Brachman D, Buckner J, Fink K, Souhami L, Laperriere N, Curran W, et al. 2013. Phase III trial of chemoradiotherapy for anaplastic oligodendroglioma: Long-term results of RTOG 9402. J Clin Oncol 31(3):337-43.

Cervera P, Videau C, Viollet C, Petrucci C, Lacombe J, Winsky-Sommerer R, Csaba Z, Helboe L, Daumas-Duport C, Reubi JC, et al. 2002. Comparison of somatostatin receptor expression in human gliomas and medulloblastomas. J Neuroendocrinol 14(6):458-71.

Choi JH, Oh JY, Ryu SK, Kim SJ, Lee NY, Kim YS, Yi SY, Shim KS, Han WS. 1997. Detection of epidermal growth factor receptor in the serum of gastric carcinoma patients. Cancer 79(10):1879-83.

Cole SL and Schindler M. 2000. Characterisation of somatostatin sst2 receptor splice variants. J Physiol Paris 94(3-4):217-37.

Cuddapah VA, Robel S, Watkins S, Sontheimer H. 2014. A neurocentric perspective on glioma invasion. Nat Rev Neurosci 15(7):455-65.

Dutour A, Kumar U, Panetta R, Ouafik L, Fina F, Sasi R, Patel YC. 1998. Expression of somatostatin receptor subtypes in human brain tumors. Int J Cancer 76(5):620-27.

ElBanan MG, Amer AM, Zinn PO, Colen RR. 2015. Imaging genomics of glioblastoma: State of the art bridge between genomics and neuroradiology. Neuroimaging Clin N Am 25(1):141-53.

Eriksson B, Kloppel G, Krenning E, Ahlman H, Plockinger U, Wiedenmann B, Arnold R, Auernhammer C, Korner M, Rindi G, et al. 2008. Consensus guidelines for the management of patients with digestive neuroendocrine tumors--well-differentiated jejunal-ileal tumor/carcinoma. Neuroendocrinology 87(1):8-19.

Fischer T, Doll C, Jacobs S, Kolodziej A, Stumm R, Schulz S. 2008. Reassessment of sst2 somatostatin receptor expression in human normal and neoplastic tissues using the novel rabbit monoclonal antibody UMB-1. J Clin Endocrinol Metab 93(11):4519-24.

Focus Oncologiae. 2011. Aivokasvaimet. syöpäsäätiön julkaisusarja. 12.

Gaafar R, Bahnassy A, Abdelsalam I, Kamel MM, Helal A, Abdel-Hamid A, Eldin NA, Mokhtar N. 2010. Tissue and serum EGFR as prognostic factors in malignant pleural mesothelioma. Lung Cancer 70(1):43-50.

Gains JE, Bomanji JB, Fersht NL, Sullivan T, D'Souza D, Sullivan KP, Aldridge M, Waddington W, Gaze MN. 2011. ^{177}Lu-DOTATATE molecular radiotherapy for childhood neuroblastoma. J Nucl Med 52(7):1041-47.

Galldiks N, Langen KJ, Pope WB. 2015. From the clinician's point of view - what is the status quo of positron emission tomography in patients with brain tumors? Neuro Oncol 17(11):1434-44.

Gorlia T, Delattre JY, Brandes AA, Kros JM, Taphoorn MJ, Kouwenhoven MC, Bernsen HJ, Frenay M, Tijssen CC, Lacombe D, et al. 2013. New clinical, pathological and molecular prognostic models and calculators in patients with locally diagnosed anaplastic oligodendroglioma or oligoastrocytoma. A prognostic factor analysis of European Organisation for Research and Treatment of Cancer Brain Tumour Group Study 26951. Eur J Cancer 49(16):3477-85.

Haldemann AR, Rosler H, Barth A, Waser B, Geiger L, Godoy N, Markwalder RV, Seiler RW, Sulzer M, Reubi JC. 1995. Somatostatin receptor scintigraphy in central nervous system tumors: Role of blood-brain barrier permeability. J Nucl Med 36(3):403-10.

Hanscheid H, Sweeney RA, Flentje M, Buck AK, Lohr M, Samnick S, Kreissl M, Verburg FA. 2012. PET SUV correlates with radionuclide uptake in peptide receptor therapy in meningioma. Eur J Nucl Med Mol Imaging 39(8):1284-88.

Hartmann C, Hentschel B, Wick W, Capper D, Felsberg J, Simon M, Westphal M, Schackert G, Meyermann R, Pietsch T, et al. 2010. Patients with IDH1 wild type anaplastic astrocytomas exhibit worse prognosis than IDH1-mutated glioblastomas, and IDH1 mutation status accounts for the unfavorable prognostic effect of higher age: Implications for classification of gliomas. Acta Neuropathol 120(6):707-18.

Hartmann C, Meyer J, Balss J, Capper D, Mueller W, Christians A, Felsberg J, Wolter M, Mawrin C, Wick W, et al. 2009. Type and frequency of IDH1 and IDH2 mutations are related to astrocytic and oligodendroglial differentiation and age: A study of 1,010 diffuse gliomas. Acta Neuropathol 118(4):469-74.

Heaphy CM, de Wilde RF, Jiao Y, Klein AP, Edil BH, Shi C, Bettegowda C, Rodriguez FJ, Eberhart CG, Hebbar S, et al. 2011. Altered telomeres in tumors with ATRX and DAXX mutations. Science 333(6041):425.

Hegi ME, Rajakannu P, Weller M. 2012. Epidermal growth factor receptor: A re-emerging target in glioblastoma. Curr Opin Neurol 25(6):774-79.

Hegi ME, Diserens AC, Gorlia T, Hamou MF, de Tribolet N, Weller M, Kros JM, Hainfellner JA, Mason W, Mariani L, et al. 2005. MGMT gene silencing and benefit from temozolomide in glioblastoma. N Engl J Med 352(10):997-1003.

Henson JW, Gaviani P, Gonzalez RG. 2005. MRI in treatment of adult gliomas. Lancet Oncol 6(3):167-75.

Herrmann M, Vos P, Wunderlich MT, de Bruijn CH, Lamers KJ. 2000. Release of glial tissue-specific proteins after acute stroke: A comparative analysis of serum concentrations of protein S-100B and glial fibrillary acidic protein. Stroke 31(11):2670-77.

Heute D, Kostron H, von Guggenberg E, Ingorokva S, Gabriel M, Dobrozemsky G, Stockhammer G, Virgolini IJ. 2010. Response of recurrent high-grade glioma to treatment with (90)Y-DOTATOC. J Nucl Med 51(3):397-400.

Higano S, Yun X, Kumabe T, Watanabe M, Mugikura S, Umetsu A, Sato A, Yamada T, Takahashi S. 2006. Malignant astrocytic tumors: Clinical importance of apparent diffusion coefficient in prediction of grade and prognosis. Radiology 241(3):839-46.

Hofman MS, Lau WF, Hicks RJ. 2015. Somatostatin receptor imaging with ^{68}Ga DOTATATE PET/CT: Clinical utility, normal patterns, pearls, and pitfalls in interpretation. Radiographics 35(2):500-16.

Horbinski C. 2013. What do we know about IDH1/2 mutations so far, and how do we use it? Acta Neuropathol 125(5):621-36.

Husain H, Savage W, Grossman SA, Ye X, Burger PC, Everett A, Bettegowda C, Diaz LA,Jr, Blair C, Romans KE, et al. 2012. Pre- and post-operative plasma glial fibrillary acidic protein levels in patients with newly diagnosed gliomas. J Neurooncol 109(1):123-27.

Hygino da Cruz LC,Jr, Rodriguez I, Domingues RC, Gasparetto EL, Sorensen AG. 2011. Pseudoprogression and pseudoresponse: Imaging challenges in the assessment of posttreatment glioma. AJNR Am J Neuroradiol 32(11):1978-85.

Jung CS, Foerch C, Schanzer A, Heck A, Plate KH, Seifert V, Steinmetz H, Raabe A, Sitzer M. 2007. Serum GFAP is a diagnostic marker for glioblastoma multiforme. Brain 130(Pt 12):3336-41.

Kabasakal L, Demirci E, Ocak M, Decristoforo C, Araman A, Ozsoy Y, Uslu I, Kanmaz B. 2012. Comparison of (68)ga-DOTATATE and (68)ga-DOTANOC PET/CT imaging in the same patient group with neuroendocrine tumours. Eur J Nucl Med Mol Imaging 39(8):1271-77.

Kamoun A, Idbaih A, Dehais C, Elarouci N, Carpentier C, Letouze E, Colin C, Mokhtari K, Jouvet A, Uro-Coste E, et al. 2016. Integrated multi-omics analysis of oligodendroglial tumours identifies three subgroups of 1p/19q co-deleted gliomas. Nat Commun 7:11263.

Kegelman TP, Hu B, Emdad L, Das SK, Sarkar D, Fisher PB. 2014. In vivo modeling of malignant glioma: The road to effective therapy. Adv Cancer Res 121:261-330.

Kloosterhof NK, Bralten LB, Dubbink HJ, French PJ, van den Bent MJ. 2011. Isocitrate dehydrogenase-1 mutations: A fundamentally new understanding of diffuse glioma? Lancet Oncol 12(1):83-91.

Korner M, Waser B, Schonbrunn A, Perren A, Reubi JC. 2012. Somatostatin receptor subtype 2A immunohistochemistry using a new monoclonal antibody selects tumors suitable for in vivo somatostatin receptor targeting. Am J Surg Pathol 36(2):242-52.

Laerum OD and Rajewsky MF. 1975. Neoplastic transformation of fetal rat brain cells in culture after exposure to ethylnitrosourea in vivo. J Natl Cancer Inst 55(5):1177-87.

Lamberts SW, van der Lely AJ, de Herder WW, Hofland LJ. 1996. Octreotide. N Engl J Med 334(4):246-54.

Li XG, Helariutta K, Roivainen A, Jalkanen S, Knuuti J, Airaksinen AJ. 2014. Using 5-deoxy-5-[18F]fluororibose to glycosylate peptides for positron emission tomography. Nat Protoc 9(1):138-45.

Lin LC and Sibille E. 2013. Reduced brain somatostatin in mood disorders: A common pathophysiological substrate and drug target? Front Pharmacol 4:110.

Loimaala A, Mäenpää H, Lipponen T, Schildt J, Kämäräinen EL, Karhumäki L, Ahonen A. 2014. ^{68}Ga-DOTA-PET for neuroendocrine tumours. Duodecim 130(19):1931-38.

Louis DN, Ohgaki H, Wiestler OD, Cavenee WK, Burger PC, Jouvet A, Scheithauer BW, Kleihues P. 2007. The 2007 WHO classification of tumours of the central nervous system. Acta Neuropathol 114(2):97-109.

Louis DN, Perry A, Reifenberger G, von Deimling A, Figarella-Branger D, Cavenee WK, Ohgaki H, Wiestler OD, Kleihues P, Ellison DW. 2016. The 2016 World Health Organization Classification of Tumors of the Central Nervous System: A summary. Acta Neuropathol 131(6):803-20.

Maecke HR and Reubi JC. 2011. Somatostatin receptors as targets for nuclear medicine imaging and radionuclide treatment. J Nucl Med 52(6):841-44.

Martin V, Mazzucchelli L, Frattini M. 2009. An overview of the epidermal growth factor receptor fluorescence in situ hybridisation challenge in tumour pathology. J Clin Pathol 62(4):314-24.

Mawrin C, Schulz S, Pauli SU, Treuheit T, Diete S, Dietzmann K, Firsching R, Schulz S, Hollt V. 2004. Differential expression of sst1, sst2A, and sst3 somatostatin receptor proteins in low-grade and high-grade astrocytomas. J Neuropathol Exp Neurol 63(1):13-19.

Merlo A, Hausmann O, Wasner M, Steiner P, Otte A, Jermann E, Freitag P, Reubi JC, Muller-Brand J, Gratzl O, et al. 1999. Locoregional regulatory peptide receptor targeting with the diffusible somatostatin analogue 90Y-labeled DOTA0-D-Phe1-Tyr3-octreotide (DOTATOC): A pilot study in human gliomas. Clin Cancer Res 5(5):1025-33.

Miederer M, Seidl S, Buck A, Scheidhauer K, Wester HJ, Schwaiger M, Perren A. 2009. Correlation of immunohistopathological expression of somatostatin receptor 2 with standardised uptake values in ^{68}Ga-DOTATOC PET/CT. Eur J Nucl Med Mol Imaging 36(1):48-52.

Mittra E and Quon A. 2009. Positron emission tomography/computed tomography: The current technology and applications. Radiol Clin North Am 47(1):147-60.

Mohammadzadeh A, Mohammadzadeh V, Kooraki S, Sotoudeh H, Kadivar S, Shakiba M, Rasuli B, Borhani A, Mohammadzadeh M. 2016. Pretreatment evaluation of glioma. Neuroimaging Clin N Am 26(4):567-80.

Mussig K, Oksuz MO, Dudziak K, Ueberberg B, Wehrmann M, Horger M, Schulz S, Haring HU, Pfannenberg C, Bares R, et al. 2010. Association of somatostatin receptor 2 immunohistochemical expression with [111In]-DTPA octreotide scintigraphy and [68Ga]-DOTATOC PET/CT in neuroendocrine tumors. Horm Metab Res 42(8):599-606.

Nyuyki F, Plotkin M, Graf R, Michel R, Steffen I, Denecke T, Geworski L, Fahdt D, Brenner W, Wurm R. 2010. Potential impact of (68)ga-DOTATOC PET/CT on stereotactic radiotherapy planning of meningiomas. Eur J Nucl Med Mol Imaging 37(2):310-18.

Oh MJ, Choi JH, Kim IH, Lee YH, Huh JY, Park YK, Lee KW, Chough SY, Joo KS, Ku BS, et al. 2000. Detection of epidermal growth factor receptor in the serum of patients with cervical carcinoma. Clin Cancer Res 6(12):4760-63.

Ohgaki H and Kleihues P. 2007. Genetic pathways to primary and secondary glioblastoma. Am J Pathol 170(5):1445-53.

Okamoto Y, Di Patre PL, Burkhard C, Horstmann S, Jourde B, Fahey M, Schuler D, Probst-Hensch NM, Yasargil MG, Yonekawa Y, et al. 2004. Population-based study on incidence, survival rates, and genetic alterations of low-grade diffuse astrocytomas and oligodendrogliomas. Acta Neuropathol 108(1):49-56.

Okuwaki K, Kida M, Mikami T, Yamauchi H, Imaizumi H, Miyazawa S, Iwai T, Takezawa M, Saegusa M, Watanabe M, et al. 2013. Clinicopathologic characteristics of pancreatic neuroendocrine tumors and relation of somatostatin receptor type 2A to outcomes. Cancer 119(23):4094-102.

Ostrom QT, Gittleman H, Fulop J, Liu M, Blanda R, Kromer C, Wolinsky Y, Kruchko C, Barnholtz-Sloan JS. 2015. CBTRUS statistical report: Primary brain and central nervous system tumors diagnosed in the United States in 2008-2012. Neuro Oncol 17 Suppl 4:iv1-iv62.

Parsons DW, Jones S, Zhang X, Lin JC, Leary RJ, Angenendt P, Mankoo P, Carter H, Siu IM, Gallia GL, et al. 2008. An integrated genomic analysis of human glioblastoma multiforme. Science 321(5897):1807-12.

Patel YC, Greenwood M, Kent G, Panetta R, Srikant CB. 1993. Multiple gene transcripts of the somatostatin receptor SSTR2: Tissue-selective distribution and cAMP regulation. Biochem Biophys Res Commun 192(1):288-94.

Pozsgai E, Schally AV, Halmos G, Rick F, Bellyei S. 2010. The inhibitory effect of a novel cytotoxic somatostatin analogue AN-162 on experimental glioblastoma. Horm Metab Res 42(11):781-6.

Quaranta M, Divella R, Daniele A, Di Tardo S, Venneri MT, Lolli I, Troccoli G. 2007. Epidermal growth factor receptor serum levels and prognostic value in malignant gliomas. Tumori 93(3):275-80.

Raggi CC, Maggi M, Renzi D, Calabro A, Bagnoni ML, Scaruffi P, Tonini GP, Pazzagli M, De Bernardi B, Bernini G, et al. 2000. Quantitative determination of sst2 gene expression in neuroblastoma tumor predicts patient outcome. J Clin Endocrinol Metab 85(10):3866-73.

Reubi JC, Laissue J, Krenning E, Lamberts SW. 1992. Somatostatin receptors in human cancer: Incidence, characteristics, functional correlates and clinical implications. J Steroid Biochem Mol Biol 43(1-3):27-35.

Reubi JC, Lang W, Maurer R, Koper JW, Lamberts SW. 1987. Distribution and biochemical characterization of somatostatin receptors in tumors of the human central nervous system. Cancer Res 47(21):5758-64.

Reubi JC, Laissue JA, Waser B, Steffen DL, Hipkin RW, Schonbrunn A. 1999. Immunohistochemical detection of somatostatin sst2a receptors in the lymphatic, smooth muscular, and peripheral nervous systems of the human gastrointestinal tract: Facts and artifacts. J Clin Endocrinol Metab 84(8):2942-50.

Reubi JC, Schar JC, Waser B, Wenger S, Heppeler A, Schmitt JS, Macke HR. 2000. Affinity profiles for human somatostatin receptor subtypes SST1-SST5 of somatostatin radiotracers selected for scintigraphic and radiotherapeutic use. Eur J Nucl Med 27(3):273-82.

Reuss DE, Mamatjan Y, Schrimpf D, Capper D, Hovestadt V, Kratz A, Sahm F, Koelsche C, Korshunov A, Olar A, et al. 2015. IDH mutant diffuse and anaplastic astrocytomas have similar age at presentation and little difference in survival: A grading problem for WHO. Acta Neuropathol 129(6):867-73.

Rinne P, Hellberg S, Kiugel M, Virta J, Li XG, Käkelä M, Helariutta K, Luoto P, Liljenbäck H, Hakovirta H, et al. 2016. Comparison of somatostatin receptor 2-targeting PET tracers in the detection of mouse atherosclerotic plaques. Mol Imaging Biol 18(1):99-108.

Sadeghi N, D'Haene N, Decaestecker C, Levivier M, Metens T, Maris C, Wikler D, Baleriaux D, Salmon I, Goldman S. 2008. Apparent diffusion coefficient and cerebral blood volume in brain gliomas: Relation to tumor cell density and tumor microvessel density based on stereotactic biopsies. AJNR Am J Neuroradiol 29(3):476-82.

Schmidt KC and Smith CB. 2005. Resolution, sensitivity and precision with autoradiography and small animal positron emission tomography: Implications for functional brain imaging in animal research. Nucl Med Biol 32(7):719-25.

Schmidt M, Scheidhauer K, Luyken C, Voth E, Hildebrandt G, Klug N, Schicha H. 1998. Somatostatin receptor imaging in intracranial tumours. Eur J Nucl Med 25(7):675-86.

Schottelius M, Wester HJ, Reubi JC, Senekowitsch-Schmidtke R, Schwaiger M. 2002. Improvement of pharmacokinetics of radioiodinated tyr(3)-octreotide by conjugation with carbohydrates. Bioconjug Chem 13(5):1021-30.

Schumacher T, Hofer S, Eichhorn K, Wasner M, Zimmerer S, Freitag P, Probst A, Gratzl O, Reubi JC, Maecke R, et al. 2002. Local injection of the 90Y-labelled peptidic vector DOTATOC to control gliomas of WHO grades II and III: An extended pilot study. Eur J Nucl Med Mol Imaging 29(4):486-93.

Seystahl K, Stoecklein V, Schuller U, Rushing E, Nicolas G, Schafer N, Ilhan H, Pangalu A, Weller M, Tonn JC, et al. 2016. Somatostatin receptor-targeted radionuclide therapy for progressive meningioma: Benefit linked to ^{68}Ga-DOTATATE/-TOC uptake. Neuro Oncol 18(11):1538-47.

Sharma P, Mukherjee A, Bal C, Malhotra A, Kumar R. 2013. Somatostatin receptor-based PET/CT of intracranial tumors: A potential area of application for 68 ga-DOTA peptides? AJR Am J Roentgenol 201(6):1340-47.

Shinojima N, Tada K, Shiraishi S, Kamiryo T, Kochi M, Nakamura H, Makino K, Saya H, Hirano H, Kuratsu J, et al. 2003. Prognostic value of epidermal growth factor receptor in patients with glioblastoma multiforme. Cancer Res 63(20):6962-70.

Soffietti R, Baumert BG, Bello L, von Deimling A, Duffau H, Frenay M, Grisold W, Grant R, Graus F, Hoang-Xuan K, et al. 2010. Guidelines on management of low-grade gliomas: Report of an EFNS-EANO task force. Eur J Neurol 17(9):1124-33.

Sottoriva A, Spiteri I, Piccirillo SG, Touloumis A, Collins VP, Marioni JC, Curtis C, Watts C, Tavare S. 2013. Intratumor heterogeneity in human glioblastoma reflects cancer evolutionary dynamics. Proc Natl Acad Sci U S A 110(10):4009-14.

Stupp R, Mason WP, van den Bent MJ, Weller M, Fisher B, Taphoorn MJ, Belanger K, Brandes AA, Marosi C, Bogdahn U, et al. 2005. Radiotherapy plus concomitant and adjuvant temozolomide for glioblastoma. N Engl J Med 352(10):987-96.

Theodoropoulou M and Stalla GK. 2013. Somatostatin receptors: From signaling to clinical practice. Front Neuroendocrinol 34(3):228-52.

Thorsen F, Ersland L, Nordli H, Enger PO, Huszthy PC, Lundervold A, Standnes T, Bjerkvig R, Lund-Johansen M. 2003. Imaging of experimental rat gliomas using a clinical MR scanner. J Neurooncol 63(3):225-31.

Tichy J, Spechtmeyer S, Mittelbronn M, Hattingen E, Rieger J, Senft C, Foerch C. 2016. Prospective evaluation of serum glial fibrillary acidic protein (GFAP) as a diagnostic marker for glioblastoma. J Neurooncol 126(2):361-69.

Tieleman A, Deblaere K, Van Roost D, Van Damme O, Achten E. 2009. Preoperative fMRI in tumour surgery. Eur Radiol 19(10):2523-34.

Tuononen K, Tynninen O, Sarhadi VK, Tyybäkinoja A, Lindlöf M, Antikainen M, Näpänkangas J, Hirvonen A, Mäenpää H, Paetau A, et al. 2012. The hypermethylation of the O6-methylguanine-DNA methyltransferase gene promoter in gliomas--correlation with array comparative genome hybridization results and IDH1 mutation. Genes Chromosomes Cancer 51(1):20-29.

Tyynelä, Sandmair A, Turunen M, Vanninen R, Vainio P, Kauppinen R, Johansson R, Vapalahti M, Ylä-Herttuala. 2002. Adenovirus-mediated herpes simplex virus thymidine kinase gene therapy in BT4C rat glioma model. Cancer Gene Ther 9(11):917-24.

van den Bent MJ, Brandes AA, Taphoorn MJ, Kros JM, Kouwenhoven MC, Delattre JY, Bernsen HJ, Frenay M, Tijssen CC, Grisold W, et al. 2013. Adjuvant procarbazine, lomustine, and vincristine chemotherapy in newly diagnosed anaplastic oligodendroglioma: Long-term follow-up of EORTC brain tumor group study 26951. J Clin Oncol 31(3):344-50.

Vanetti M, Kouba M, Wang X, Vogt G, Hollt V. 1992. Cloning and expression of a novel mouse somatostatin receptor (SSTR2B). FEBS Lett 311(3):290-94.

Velikyan I, Sundin A, Sörensen J, Lubberink M, Sandström M, Garske-Roman U, Lundqvist H, Granberg D, Eriksson B. 2014. Quantitative and qualitative intrapatient comparison of ^{68}Ga-DOTATOC and ^{68}Ga-DOTATATE: Net uptake rate for accurate quantification. J Nucl Med 55(2):204-10.

Vernejoul F, Faure P, Benali N, Calise D, Tiraby G, Pradayrol L, Susini C, Buscail L. 2002. Antitumor effect of in vivo somatostatin receptor subtype 2 gene transfer in primary and metastatic pancreatic cancer models. Cancer Res 62(21):6124-31.

Videau C, Hochgeschwender U, Kreienkamp HJ, Brennan MB, Viollet C, Richter D, Epelbaum J. 2003. Characterisation of [125I]-Tyr0DTrp8-somatostatin binding in sst1- to sst4- and SRIF-gene-invalidated mouse brain. Naunyn Schmiedebergs Arch Pharmacol 367(6):562-71.

Viollet C, Lepousez G, Loudes C, Videau C, Simon A, Epelbaum J. 2008. Somatostatinergic systems in brain: Networks and functions. Mol Cell Endocrinol 286(1-2):75-87.

Virgolini I, Ambrosini V, Bomanji JB, Baum RP, Fanti S, Gabriel M, Papathanasiou ND, Pepe G, Oyen W, De Cristoforo C, et al. 2010. Procedure guidelines for PET/CT tumour imaging with 68Ga-DOTA-conjugated peptides: 68Ga-DOTA-TOC, 68Ga-DOTA-NOC, 68Ga-DOTA-TATE. Eur J Nucl Med Mol Imaging 37(10):2004-10.

Vos PE, Jacobs B, Andriessen TM, Lamers KJ, Borm GF, Beems T, Edwards M, Rosmalen CF, Vissers JL. 2010. GFAP and S100B are biomarkers of traumatic brain injury: An observational cohort study. Neurology 75(20):1786-93.

Waser B, Tamma ML, Cescato R, Maecke HR, Reubi JC. 2009. Highly efficient in vivo agonist-induced internalization of sst2 receptors in somatostatin target tissues. J Nucl Med 50(6):936-41.

Weller M, van den Bent M, Hopkins K, Tonn JC, Stupp R, Falini A, Cohen-Jonathan-Moyal E, Frappaz D, Henriksson R, Balana C, et al. 2014. EANO guideline for the diagnosis and treatment of anaplastic gliomas and glioblastoma. Lancet Oncol 15(9):e395-403.

Wick W, Meisner C, Hentschel B, Platten M, Schilling A, Wiestler B, Sabel MC, Koeppen S, Ketter R, Weiler M, et al. 2013. Prognostic or predictive value of MGMT promoter methylation in gliomas depends on IDH1 mutation. Neurology 81(17):1515-22.

Wiestler B, Capper D, Holland-Letz T, Korshunov A, von Deimling A, Pfister SM, Platten M, Weller M, Wick W. 2013. ATRX loss refines the classification of anaplastic gliomas and identifies a subgroup of IDH mutant astrocytic tumors with better prognosis. Acta Neuropathol 126(3):443-51.

Wild D, Schmitt JS, Ginj M, Macke HR, Bernard BF, Krenning E, De Jong M, Wenger S, Reubi JC. 2003. DOTA-NOC, a high-affinity ligand of somatostatin receptor subtypes 2, 3 and 5 for labelling with various radiometals. Eur J Nucl Med Mol Imaging 30(10):1338-47.

Ålgars A, Lintunen M, Carpen O, Ristamäki R, Sundström J. 2011. EGFR gene copy number assessment from areas with highest EGFR expression predicts response to anti-EGFR therapy in colorectal cancer. Br J Cancer 105(2):255-62.

Annales Universitatis Turkuensis

Turun yliopisto
University of Turku

Painosalama Oy, Turku, Finland 2017

ISBN 978-951-29-6814-5 (PRINT)
ISBN 978-951-29-6815-2 (PDF)
ISSN 0355-9483 (Print) | ISSN 2343-3213 (Online)